

Perturbed orbital motion of regolith around Asteroids

MSc Thesis Report

Abhishek Agrawal



Cover image credit: Adopted from European Southern Observatory. Artist's Impression of the binary asteroid Antiope.

"If you wish to make an apple pie from scratch, you must first invent the universe."

Carl Sagan

PREFACE

After 45 years since the day man landed on the Moon, mankind created history, yet again. For the first time ever, a spacecraft was put into an orbit around a comet and a lander was deployed to its surface. This was the Rosetta mission; launched in March 2004, the spacecraft took an astonishing 10 years to travel to the comet 67P/Churyumov-Gerasimenko, finally arriving at the comet in August 2014. This is an immense achievement for the scientists and engineers involved in the Rosetta mission because space missions to small irregular bodies in our solar system, both comets and asteroids, pose significant dynamical challenges. For scientists, missions to comets and asteroids are of great interest since in-situ exploration of these small bodies can provide insight into the birth of our Solar System and answer some very important and fundamental questions such as those about the origins of life on Earth. Now even the private space industry is interested in these small bodies, such as in mining the vast reserves of untapped natural resources within the small bodies. For a student, designing and assessing orbits around a small irregular body, and in our case an asteroid, turns out to be one of the toughest problems in astrodynamics, making it a perfect research topic for an MSc Thesis.

This report serves to be a *Literature Study* in the framework of the Master's program at the Faculty of Aerospace Engineering, Delft University of Technology. It paves way for the upcoming thesis project, where the actual research work shall be carried out. I am grateful I could do this literature study under the supervision of my supervisor Ir. Ron Noomen and with support from Dr. Jinglang Feng. Their experience in the subject matter has been of tremendous help to me. In writing this report, I have tried my very best to ensure that the material in the report is presented in a manner which is pleasant to read and understand. I hope you can gain some valuable knowledge from reading this report.

*Abhishek Agrawal
Delft, August 2016*

CONTENTS

Preface	v
List of Symbols	ix
List of Acronyms	xi
1 Introduction	1
1.1 Research problem	3
1.2 Structure of the report	3
2 Results	5
2.1 Regolith launched from the longest edge of the asteroid	5
2.1.1 Dynamics without Solar perturbations	5
2.1.2 Dynamics with Solar perturbations	5
Bibliography	27
Appendices	29
A Extra Figures	31

LIST OF SYMBOLS

LATIN LETTERS

Symbol	Units	Description
r	m	position vector magnitude
\mathbf{r}	m	position vector
U	m^2/s^2	Gravitational potential

GREEK

Symbol	Units	Description
α	m	Largest semi-major axis of tri-axial ellipsoid shaped asteroid

LIST OF ACRONYMS

AU	Astronomical Unit
CCW	Counter-Clockwise
MBO	Main-Belt Objects
NEA	Near-Earth Asteroids
SRP	Solar Radiation Pressure
STBE	Solar Third Body Effect
TNO	Trans-Neptunian Objects

1

INTRODUCTION

Asteroids are small rocky bodies in our solar system that are orbiting the Sun. These small bodies are basically the remnants from the process that formed the inner planets in our Solar System [3]. Asteroids are mainly found in an orbit between Jupiter and Mars and as such are classified as MBO (Main-Belt Objects). These MBO range in size from a few meters to hundreds of kilometers, the largest one being 1 Ceres with a diameter of 948 km. A subset of the MBO, called the NEA (Near-Earth Asteroids), are asteroids whose orbits come extremely close to, and sometimes even cross, the orbit of the Earth [2]. Other small bodies in our small system, classified as asteroids when broadly speaking, are the Trojans (small bodies captured at Jupiter's Lagrange points 4 and 5), the TNO (Trans-Neptunian Objects) (small bodies whose orbits around the Sun go beyond Neptune), the Centaurs (small bodies whose orbits lie in between Jupiter and Neptune) [2]. The asteroids in the main-belt tend to be more rocky in nature, however the small bodies beyond Jupiter tend to have a more icy-composition due to their relatively larger distance from the Sun [2]. A histogram plot depicting the distribution of MBO is shown in Figure 1.1. The gaps in the plot depict resonance in mean-motion between Jupiter and an asteroid [2].

Asteroids don't only exist as single bodies in the Solar System, but they are also found in local multi-body systems consisting of two to even three asteroids. With advanced asteroid detection methods, astrophysicists have found over 190 multiple asteroid systems in the Solar System [5]. Contrary to intuition, these multiple asteroid systems exhibit a wide diversity in terms of the size ratios of the components, their mutual orbits and separation, implicating that the individual components evolved differently over time [5]. If a multi-asteroid system consists of two or three components, which are bound gravitationally, then it is termed as *binary asteroids* or *triple asteroids* respectively. Triple asteroids are also sometimes termed as *trinary* or *ternary* [6]. Asteroid components that are not gravitationally bound but are genetically related, are termed as *asteroid pairs*. Asteroid pairs where the larger asteroid is a binary or a triple asteroid, are termed as *paired binaries* or *paired triples*, respectively. The larger component in a binary or triple asteroid system or an asteroid pair, is referred to as the *primary* and similarly the smaller component is referred to as the *secondary* [6]. Asteroids are further classified based on their dimensions and thermal properties, for which the reader should read the publication in [5].

We now know what asteroids are and the different ways in which they are found in our Solar System, but is it important to study them? There are three major, and most commonly expressed, reasons to study asteroids in our solar system, and not just from a distance such as through radar telescopes placed on Earth, but also through in-situ exploration involving spacecrafts and surface probes. These reasons are mentioned as follows.

- Asteroids are basically the material left-over from formation of planets in our Solar System. Thus, they are the perfect source to study and understand the origins of the Solar System, as

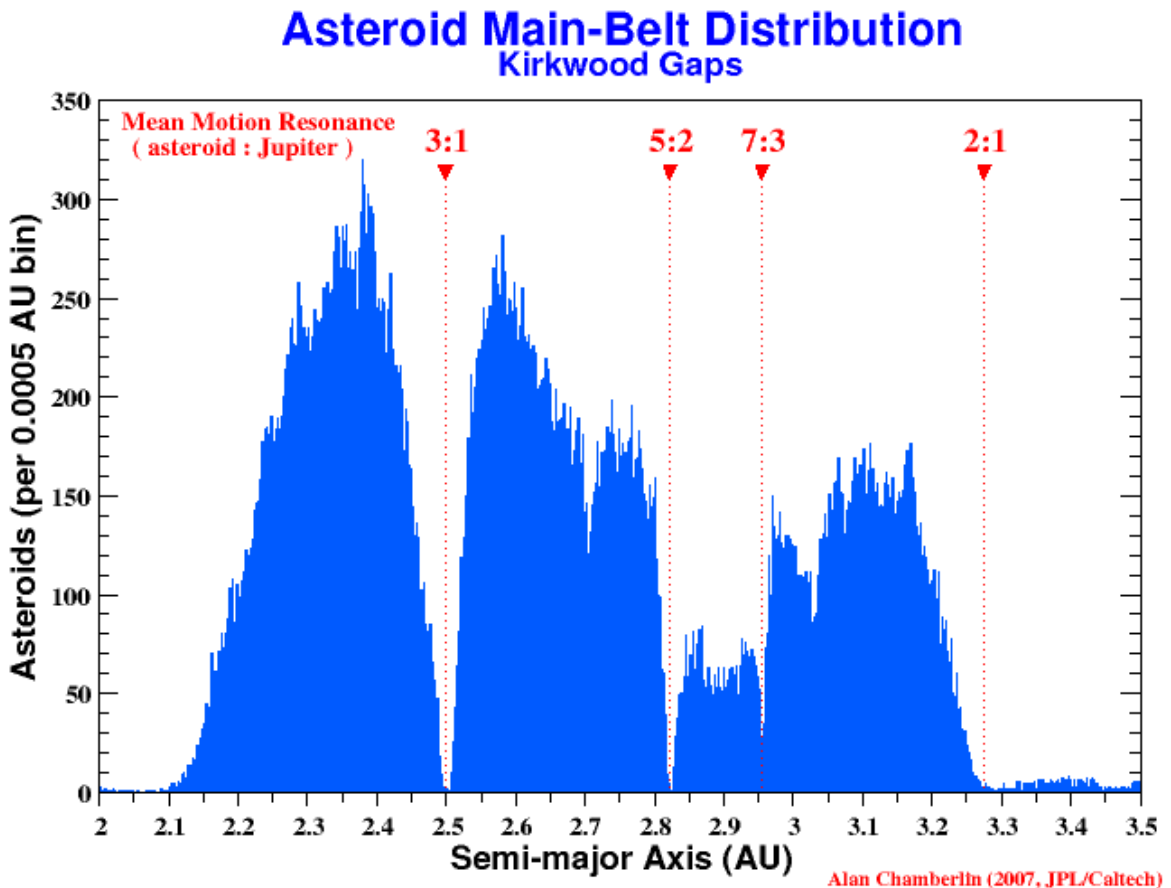


Figure 1.1: Histogram plot depicting distribution of semi-major axis of 156,929 main-belt asteroids, created in June 2007 [2].

they have remained in the same pristine form since the birth of the Solar System, unlike the planets which have undergone massive topographical and atmospheric changes after their formation. The asteroids can provide valuable information on the chemical composition and initial conditions which led to the formation of planets, including Earth some 4.6 billion years ago. Several scientists have also hypothesized that water and life could have been brought about on Earth through an asteroid or comet and hence exploration of these small bodies could provide a definite answer to an age old question of how life began on Earth [3].

- Asteroids have been hypothesized to have brought complex molecules to the surface of Earth that eventually resulted in life, but lately they have also been linked to the extinction of dinosaurs due to its impact with Earth. Earth is continuously bombarded with very small interplanetary material, most of which doesn't reach the surface of the Earth but gets evaporated in its atmosphere. However, every few 100 years, an asteroid spanning some tens of meter could impact Earth resulting in widespread damage, in the present case to life and property. But the impact from those will not cause the human race to extinct. But every 100,000 years or so, larger asteroids, spanning over tens of kilometer would impact the Earth, which will lead to extinction of life as we know it now. Although the probability of getting hit by an asteroid on such a large scale is low, it is still a statistical possibility and to be able to device strategies for active deflection of such asteroids, it is imperative that we understand more of the dynamics, properties and composition of the asteroids [3].

- The third most important reason for us to study asteroids, is the fact that these small bodies are rich in raw materials or minerals. NEA can be exploited for the resources that they possess and use it to build space structures or generate fuel for spacecrafts to enable human space exploration in farther reaches of the Solar System. By studying the asteroids, we can develop methods to tap the vast reservoirs of raw materials residing in them [3].

1.1 RESEARCH PROBLEM

1.2 STRUCTURE OF THE REPORT

2

RESULTS

2.1 REGOLITH LAUNCHED FROM THE LONGEST EDGE OF THE ASTEROID

The results that we'll discuss in this section pertain to the case of regolith launched from the longest edge of the asteroid, modeled as an ellipsoid.

2.1.1 DYNAMICS WITHOUT SOLAR PERTURBATIONS

...to be added later...

2.1.2 DYNAMICS WITH SOLAR PERTURBATIONS

In this case, the simulation accounted for perturbations from the irregular gravity field of the asteroid, the SRP (Solar Radiation Pressure), and the STBE (Solar Third Body Effect). Within this category, there are 4 distinct sets of simulations, each for a particle with different Area-to-Mass ratio. These are mentioned in Table 2.1. The material with a density of $3.2 \text{ [g/cm}^3]$ is low-density Olivine and the one with $7.5 \text{ [g/cm}^3]$ is Iron-Nickel alloy [1]. The mineral Olivine can be found on asteroids and has been discovered on asteroid Itokawa through transmission electron microscope analysis of samples returned by the Hayabusa spacecraft [4]. Iron-Nickel alloy is found to be most abundant in metallic meteorites [7].

For each of the four types of particles mentioned in Table 2.1, the initial conditions for lofting the regolith are varied in the same manner. These initial conditions are mentioned as follows. The asteroid revolves around the Sun in an equatorial circular orbit at a distance of 1.0 AU (Astronomical Unit). Four different initial Solar phase angles were considered for the simulation – 45.0, 135.0, 225.0, 315.0 [deg], to account for the four different quadrants where the Sun could be with respect to the asteroid. For each case in Table 2.1, a total of 72 particles were launched from the surface of the asteroid, each in a different direction (defined using the launch declination and azimuth angles). The launch declination angle, measured from the zenith, was kept constant at 45.0 [deg] for all the particles. The launch azimuth, measured CCW (Counter-Clockwise) from the direction pointing to north, was varied at a resolution of 5.0 [deg] starting from 0.0 [deg] all the way up to 355.0 [deg].

Table 2.1: Particle Area-to-Mass ratios

Code	Particle radius [cm]	Density [g/cm ³]	Area-to-Mass ratio [m ² /kg]
LoGSP-1	1.0	3.2	0.0234
LoGSP-2	1.0	7.5	0.01
LoGSP-3	5.0	3.2	0.0047
LoGSP-4	5.0	7.5	0.002

Each particle was launched, in their specified direction, with different velocities ranging from 1.0 [m/s] to 16.0 [m/s] (measured with respect to the asteroid-centric rotating frame) at a resolution of 1.0 [m/s]. So basically, every combination of an initial Solar phase angle, initial launch azimuth, and initial launch velocity corresponds to a unique trajectory for a single particle of a given Area-to-Mass ratio; Thus amounting to a total of 4608 unique trajectories. The simulations were subjected to run for a maximum of 270.0 [days] and were terminated earlier if a particular trajectory resulted in escape or surface re-impact.

CASE LoGSP-1

The density of the regolith was considered to be 3.2 [g/cm³] with a spherical shape of radius 1.0 [cm]. Figure 2.1 gives a distribution of particles for each of the three different final fates for the regolith i.e. capture, re-impact, and escape, for different initial launch velocities and initial Solar phase angles. Irrespective of the initial Solar phase, initial launch velocities from 1.0 to 3.0 [m/s] results in particles launched in all directions to eventually re-impact the asteroid's surface. Similarly, for initial launch velocities ranging from 14.0 to 16.0 [m/s], we see that the particles always manage to escape the gravitational attraction of the asteroid. However, there is one exception to the former statement, a single particle launched with a velocity of 14.0 [m/s] at a launch azimuth of 90.0 [deg] and at an initial Solar phase angle of 315.0 [deg], re-impacts the asteroid's surface. It is interesting to note that the launch azimuth of the particle is such that it is launched in a direction that is directly opposite to the direction of rotation of the asteroid. Launch velocities from 4.0 to 13.0 [m/s] show a mixed behavior and the final fate distribution trend does not vary drastically for different initial Solar phase angles.

The number of capture cases is far less than those for escape and re-impact. For initial Solar phase of 225.0 [deg], there are no cases of regolith being captured in orbit around the asteroid. All capture cases, arranged in order of increasing launch azimuth angle, are listed in Table 2.2. It is interesting to note that all capture cases result from when the particle is launched in a direction which is against the direction of rotation of the asteroid, bar one exception which is case index-11 in Table 2.2. The capture cases which represent symmetry in terms of the launch azimuth angle are

Table 2.2: Initial conditions that resulted in temporary orbital capture of regolith around the asteroid. Particle code LoGSP-1.

Index	Launch azimuth [deg]	Launch velocity [m/s]	Initial Solar phase angle [deg]
1	5.0	5.0	315.0
2	10.0	9.0	135.0
3	15.0	8.0	45.0
4	45.0	12.0	45.0
5	45.0	10.0	315.0
6	135.0	12.0	45.0
7	135.0	10.0	315.0
8	165.0	8.0	45.0
9	170.0	9.0	135.0
10	175.0	5.0	315.0
11	185.0	5.0	135.0

highlighted with the same color in Table 2.2. This symmetric behavior results from the combination of two factors. First, the Sun's motion relative to the asteroid is not in an inclined plane, and secondly, the particles are launched from the equatorial tip of the ellipsoid shaped asteroid, which is a point of symmetry on the ellipsoid. The capture cases will be discussed in detail a bit further ahead.

Regolith final fate histogram, Ellipsoid longest edge

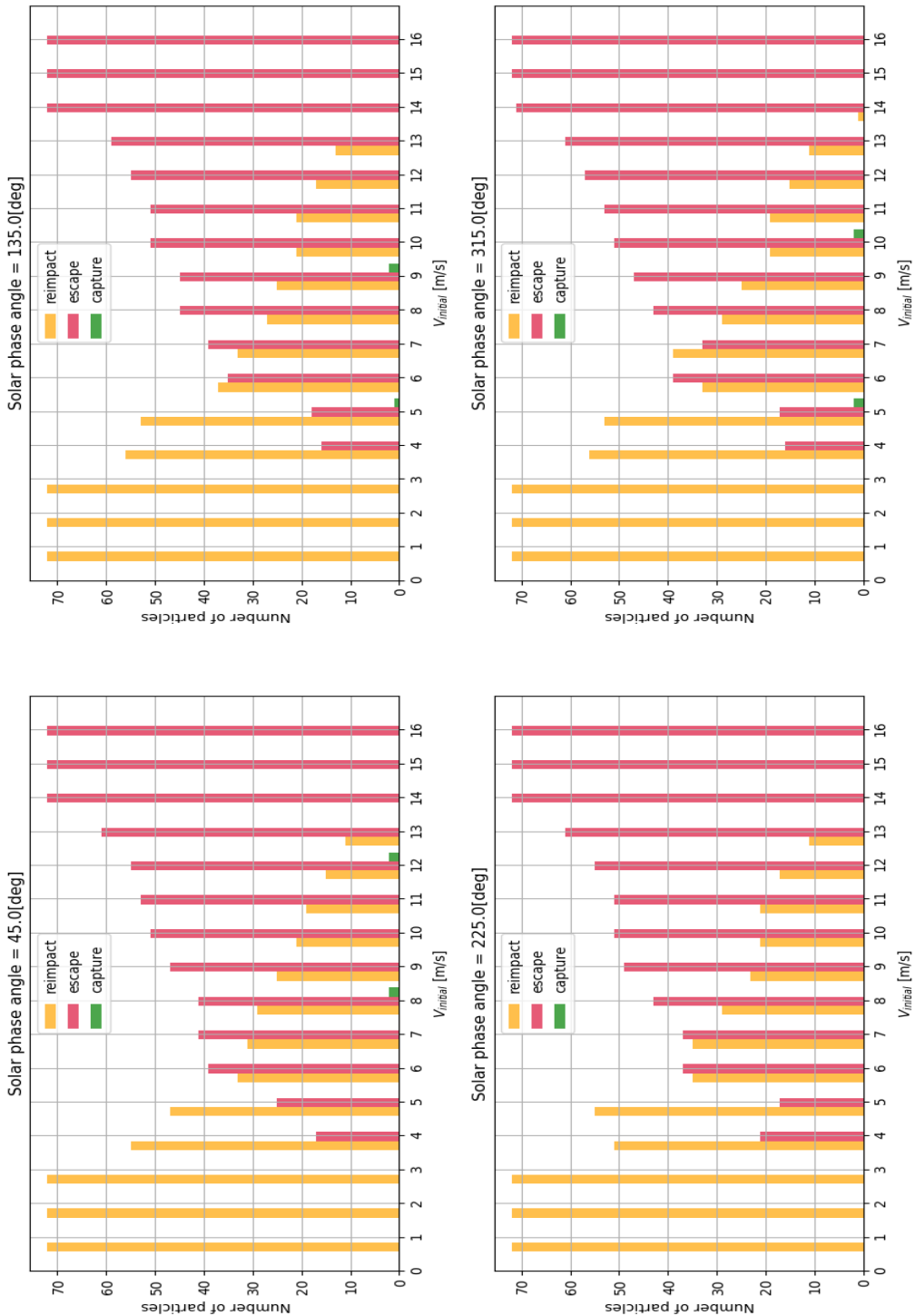


Figure 2.1: Histogram showing the number of particles that re-impact, escape, or get captured around the asteroid, for different initial launch velocities. Particle code LoGSP-1.

Figure 2.2 depicts the surface distribution of regolith that re-impacts the surface when launched from the same location with different velocities and different initial Solar phase angles. The launch location is in the centre of the map, Latitude 0.0 [deg] and Longitude 0.0 [deg]. The particle distribution is the same for regions close to the launch point and for lower launch velocities up until 8.0 [m/s]. A similarity in distribution pattern is also observed around Longitude -150.0 [deg] for launch velocity of 9.0 [m/s] and around Longitude 150.0 [deg] for launch velocity of 10.0 [m/s] for the four Solar phase angles. The distribution pattern, for all launch velocities and initial Solar phases, is also symmetric about the equator. Again, the reason for this is the same as mentioned earlier for the symmetry in capture cases in Table 2.2. Keeping the launch direction and velocity constant, we see that the distribution of regolith that re-impacts the surface does not change drastically with varying initial Solar phase angles, except for a relatively few cases. This is much easily observed in a plot of Range from the launch direction to the re-impact point versus launch azimuth for different velocities as shown in Figure 2.3.

We haven't shown the range to re-impact point plots in Figure 2.3 for all launch velocities because the intention here is to show the qualitative behavior, which can be achieved by considering only a subset of the launch velocities that result in a re-impact scenario. The very first thing we observe is that as the launch velocity increases, the range of launch azimuth over which the regolith re-impacts the surface reduces because a higher velocity allows the regolith to enter a higher orbit (as it attains a relatively higher energy) and reduces the probability of a re-impact. Even as the velocity increases, we see that the azimuths that result in a re-impact are the ones in which the regolith is launched in a direction that is opposite to the asteroid's rotation direction. This makes sense since the regolith's energy would be reduced the most in this scenario compared to all other launch directions, thereby increasing the chances of a re-impact.

Now the primary purpose of the plots in Figure 2.3 (combined with Figure 2.2) is to depict the qualitative effect of Solar perturbations, for varying initial Solar phase angles, on the re-impact behavior of regolith compared to the case when no Solar perturbations are considered. For launch velocities of 4.0, 7.0 and 10.0 [m/s], we see that the Solar perturbations do not affect the re-impact location for cases when the particle is launched in directions opposite to that of the asteroid's rotation. However, we do see few exceptions to the former statement, most noticeably in the case of 7.0 [m/s]. But for the majority of cases where the re-impact location remains unchanged, we see from Figure 2.4, that these particles spend less than 3.0 [Hrs] in orbit which is not enough time for the Solar perturbations to act and have any significant impact on the dynamics of the particles. So in essence this is what's happening here - Particles when launched in a direction that is opposite to that of the asteroid's rotation, even at relatively high velocities such as 10.0 [m/s], loose enough energy to stay in a relatively lower orbit (see Figure A.1) where the gravitational force of the asteroid is significantly stronger than any of the Solar perturbations and as the particle spends a very short time in orbit before re-impact, the Solar perturbations do not get enough time to affect the particle's orbit and hence the particle re-impacts the same location as it would have when no Solar perturbations were considered in the simulation. For the lower launch velocities of 4.0 and 7.0 [m/s], the differences in re-impact locations are more pronounced when the regolith is launched in the same direction as that of the asteroid's rotation. Particles gain relatively higher energy in this case, enter a higher orbit and spend enough time in there for the Solar perturbations to affect its motion. For the case of the launch velocity of 13.0 [m/s] in Figure 2.3, the velocity is high enough such that the particle does not loose enough energy when launched opposite to the asteroid's rotational direction and is able to enter a relatively higher orbit (see Figure A.1) and stay there for a relatively longer time, as seen in Figure 2.4, which results in the Solar perturbations affecting the orbital motion and eventually the re-impact location of the regolith.

Regolith crash map for multiple launch velocities
Ellipsoid longest edge

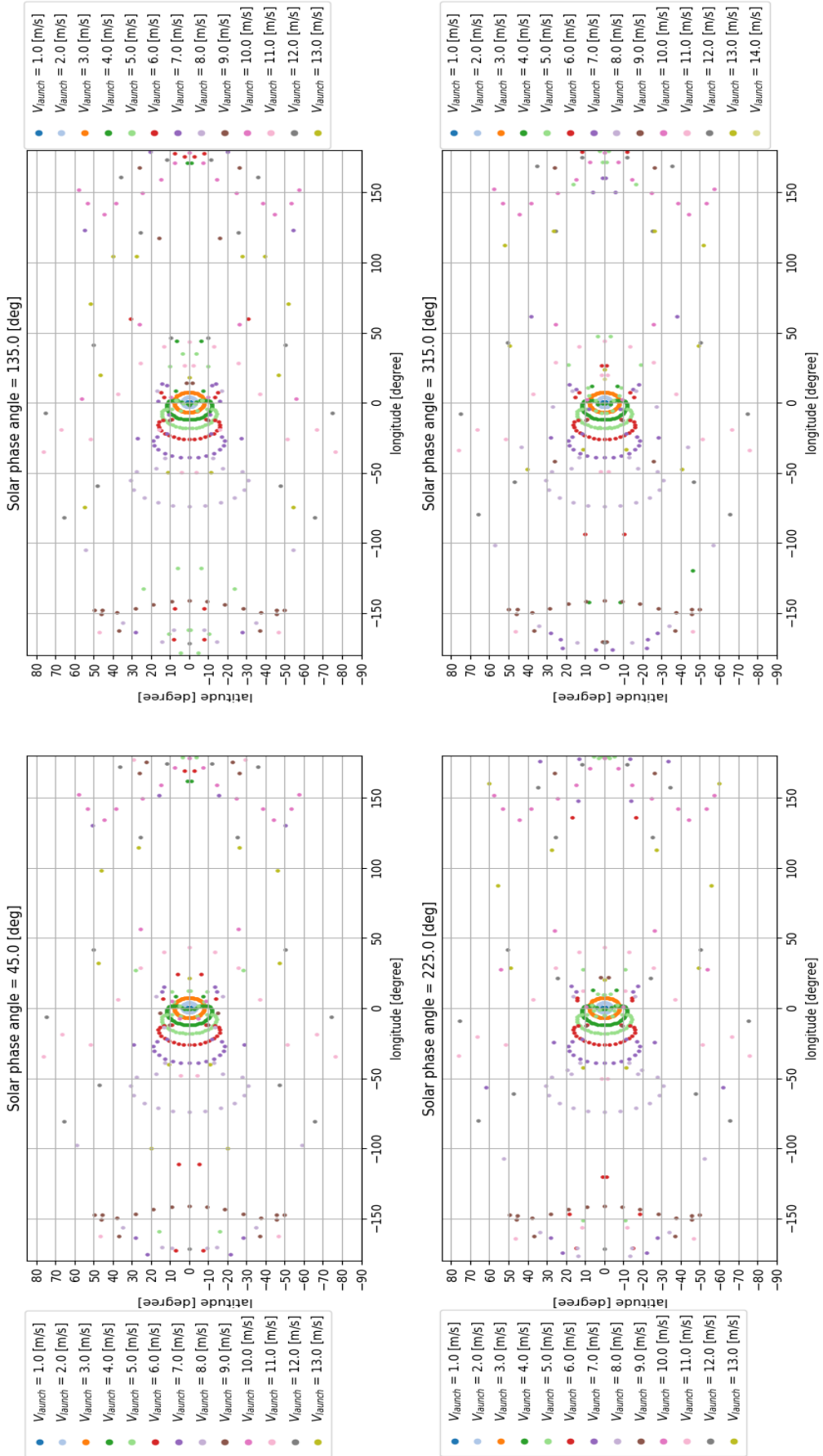


Figure 2.2: Surface distribution of re-impacted regolith for different launch velocities. The launch location is latitude: 0.0 [deg], longitude: 0.0 [deg]. Particle code LoGSP-1.

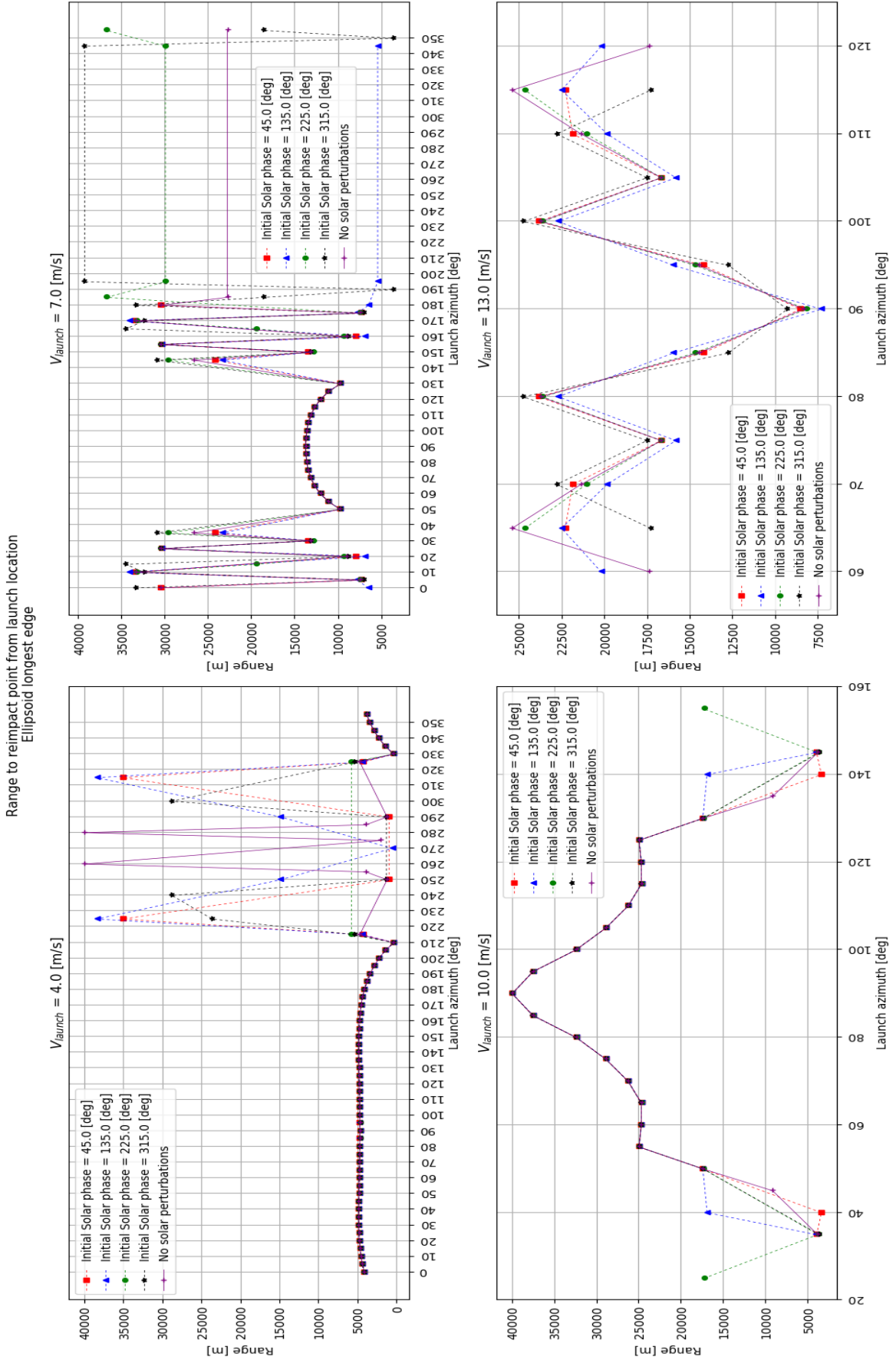
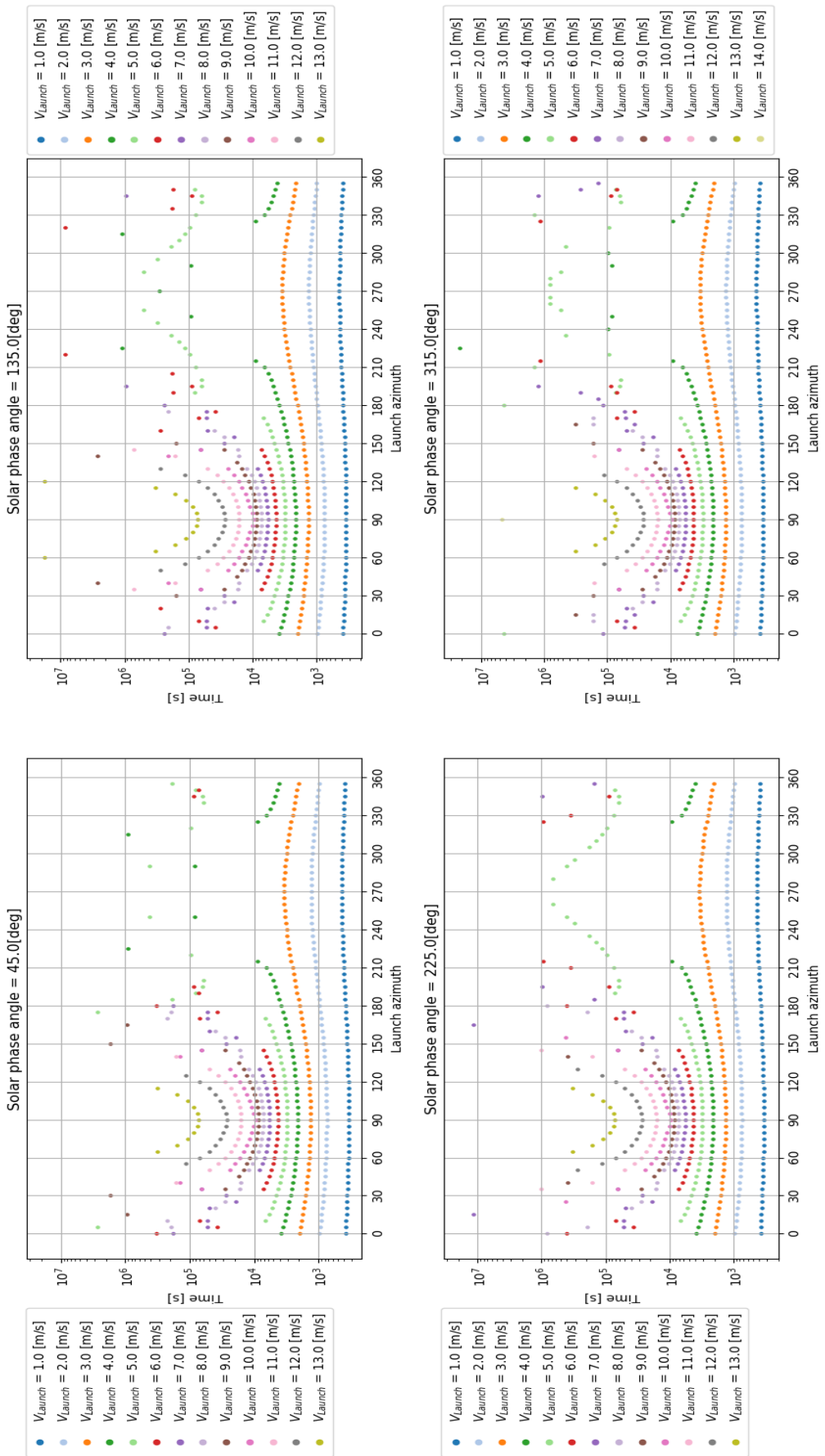


Figure 2.3: Range to re-impact location from the launch point for different velocities. Particle code LoGSP-1.

Time for regolith to reimpact; Ellipsoid Longest edge

**Figure 2.4:** Time taken by regolith at different velocities and launch directions to re-impact with the surface of the asteroid. Particle code LoGSP-1.

We shall now look at the cases where the lofted regolith gets (temporarily) captured in orbit by the asteroid. The initial conditions for all capture cases, for the current particle size and density, were mentioned earlier in Table 2.2. Figure 2.6 depicts the progression in orbital range of the temporarily captured regolith. The straight lines in the plot are used to mark the different altitude regimes. These are the LAO (Low Altitude Orbit), MAO (Medium Altitude Orbit), HAO (High Altitude Orbit), UHAO (Ultra-High Altitude Orbit), and EHAO (Extremely-High Altitude Orbit). These altitude regime definitions are not from well defined standards, but instead were arbitrarily chosen as integer multiples of the longest semi-major axis, α , of the tri-axial ellipsoid shaped asteroid. The definition for these altitude regimes is given in Table 2.3.

Table 2.3: Altitude regimes and their definitions

Altitude regime	Definition
LAO	Asteroid surface to $2 \times \alpha$
MAO	$2 \times \alpha$ to $3 \times \alpha$
HAO	$3 \times \alpha$ to $5 \times \alpha$
UHAO	$5 \times \alpha$ to $7 \times \alpha$
EHAO	Above $7 \times \alpha$

The purpose of plotting data as shown in Figure 2.6 was to look for any patterns or periodicity, if they existed, and to see if particles in temporary capture scenario remain closer to the asteroid or further away from it. The symmetry as explained for initial conditions mentioned in Table 2.2 can also be seen in Figure 2.6, for example, regolith launched with velocity of 8.0 [m/s] and launch azimuth of 15.0 [deg] (shown by the purple curve in the top plot in Figure 2.6) shows the same behavior as that of regolith launched with the same velocity and 165.0 [deg] launch azimuth (shown by the green curve in the bottom plot in Figure 2.6). Another thing we see from the plot is that, apart from case number 11 in Table 2.2, the captured regolith stay in the higher altitude regions for most part and only briefly do they fall within the MAO and LAO region. We shall now look at atleast three cases from Figure 2.6 in a bit more detail to understand the effect of Solar perturbations by comparing these cases with their counterparts from the simulation where Solar perturbations were omitted.

Of all the cases shown in Figure 2.6 or Table 2.2, the one with a launch velocity of 10.0 [m/s] and launch azimuth of 45.0 [deg] results in a re-impact scenario when Solar perturbations are omitted but the same initial conditions lead to a temporary capture orbit when perturbations were added for an initial Solar phase angle of 315.0 [deg]. Every other initial condition for the capture cases had otherwise resulted in an escape situation when simulations were conducted without the Solar perturbations. The 3D trajectory plot in two different views for the former case are shown in Figure 2.7 (see Figure A.2 also for the 3D trajectory representation in body fixed frame). The 2D trajectory for the same is shown in Figure 2.9 in inertial frame and in Figure A.3 in the asteroid centric rotating frame or the body frame. The web-link or URL for the trajectory animation of the particle (in inertial frame and in XY plane only) can be found in Figure 2.5.



Figure 2.5: 2D trajectory animation (XY Plane) of capture regolith for case number 5 in Table 2.2. Particle code LoGSP-1. Scan the QR code to view the animation or use the following web-link: <https://youtu.be/oZDhDo5CIsk>

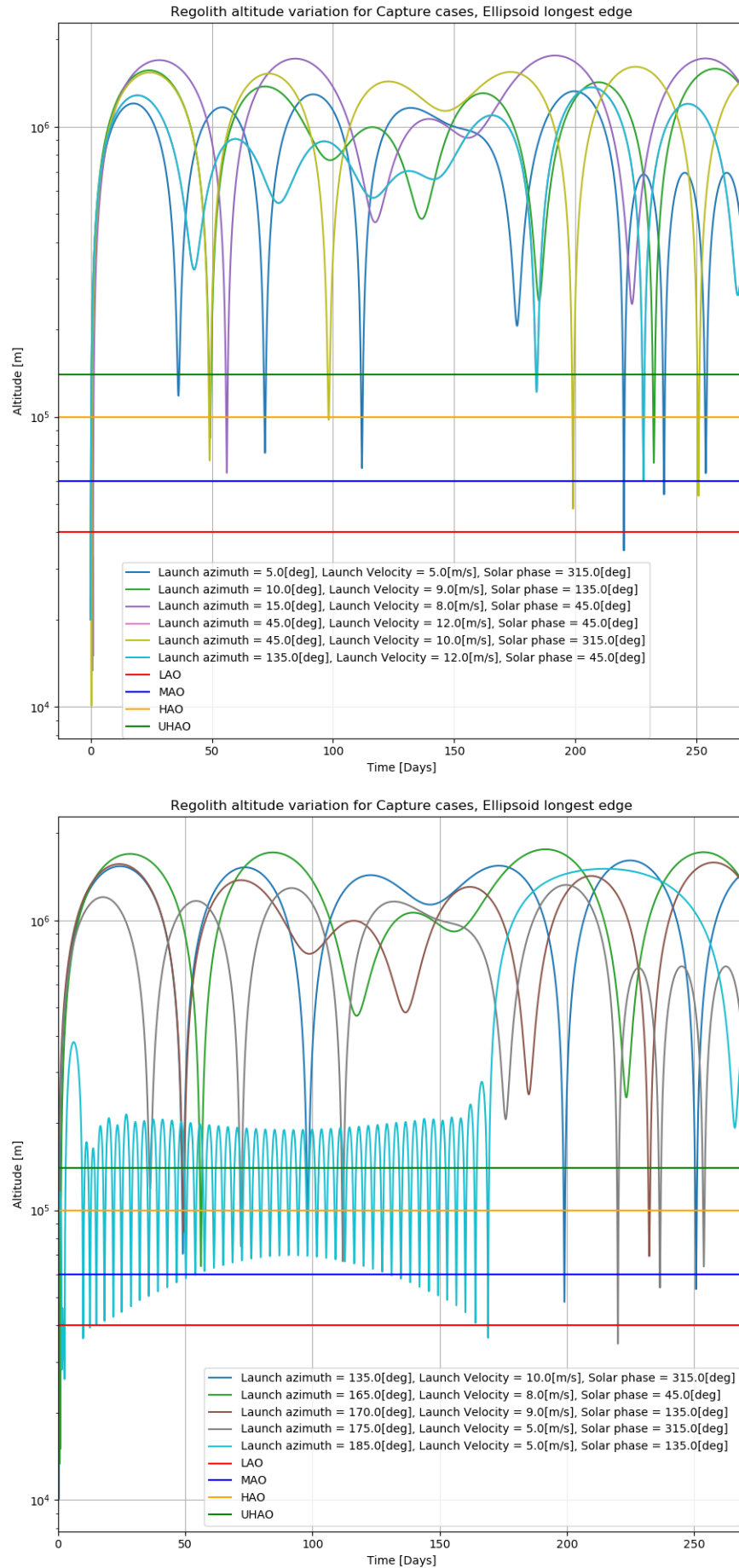


Figure 2.6: Orbital range progression with time for temporary capture scenarios. Particle code LoGSP-1.

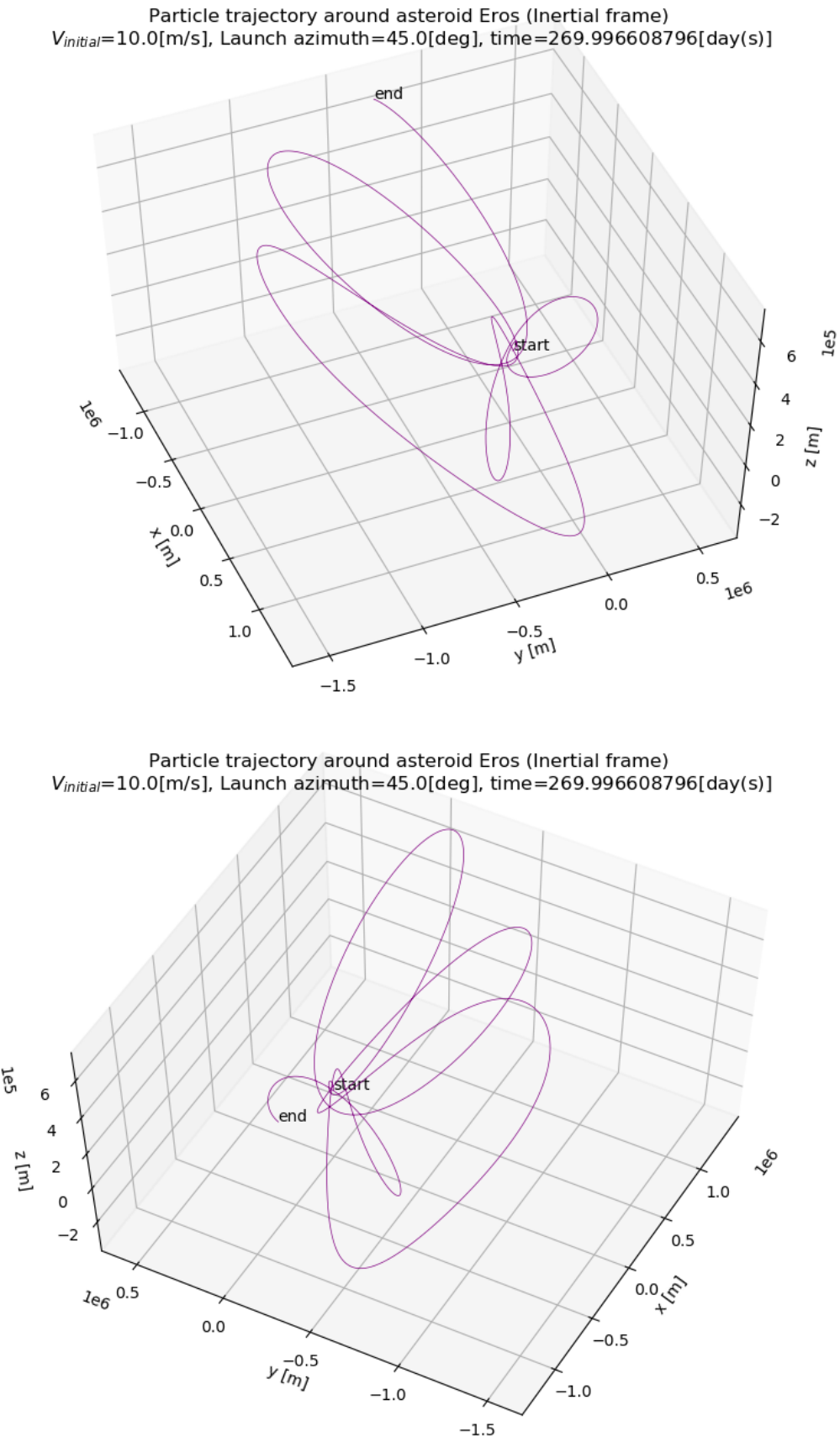


Figure 2.7: 3D inertial frame trajectory of capture regolith for case number 5 in Table 2.2 in two different viewing angles.
 Particle code LoGSP-1.

Note that in the trajectory animation in Figure 2.5 (and any other animation included henceforth) the particle is made to skip several data points in between along the trajectory when it is far away from the asteroid, just to reduce the length of the animation. So because of this, the particle appears to be moving faster when it is away from the asteroid but this is not true. For the exact velocity of the particle, the reader should look at the velocity magnitude indicator within the animation itself.

The animation shows that the particle reverses its direction of motion twice in its entire course. To visualize how this is happening in 3D, look at Figure 2.7. The reason for this can be understood by looking at the direction of the perturbing vectors in Figure 2.10. The plot shows the direction of the perturbing acceleration vector in the XY plane. Both SRP and STBE are shown separately as well as the net effect of the two. The vectors (in all three plots in Figure 2.10) are shown along those parts of the trajectory where the magnitude of SRP acceleration is of the same order of magnitude as that of the gravitational acceleration. However, the magnitude of the STBE acceleration is always 1.0 order of magnitude smaller than the gravitational acceleration for those very same points along the trajectory. The SRP is definitely more dominant of the two Solar perturbations as we can see that the direction of the net perturbation is the same as that of SRP. In the plots, the trajectory loops numbered 1 and 2, is where the particle's direction of motion reversed. And this happens because of the SRP, as the direction of the perturbation is such that it pulls the particle away from its nominal motion and forces it to change its direction. This is an interesting effect and happens only because the SRP offers an acceleration to the particle which is equally significant as the gravitational acceleration when the particle is far away from the asteroid. This is not an isolated incident and we'll show another example where this happens.

Figure 2.11 shows the 3D trajectory for completely different launch conditions (see capture case 8 in Table 2.2). The 3D trajectory as viewed from the asteroid centric body fixed frame is shown in Figure A.4. The 2D trajectory projections for the same, in inertial and body fixed frames, are shown in Figure 2.12 and Figure A.5 respectively. Just like in the previous case, we see from the animation (see Figure 2.8) and the 3D trajectory for current launch conditions that the particle direction of motion is reversed twice in its course. If we look at Figure 2.13, we see it again that the change in direction is happening because of the perturbations and more significantly by the SRP. The perturbation vectors in Figure 2.13 are plotted for points along the trajectory where the magnitude of acceleration due to SRP is of the same order of magnitude as the gravitational acceleration. Again, the magnitude of STBE is 1.0 order of magnitude smaller than the gravitational acceleration for the same data points along the trajectory. Along loops numbered 1 and 2 in Figure 2.13 the SRP direction is such that it forces the particle to change its direction of motion from its nominal course.



Figure 2.8: 2D trajectory animation (XY Plane) of capture regolith for case number 8 in Table 2.2. Particle code LoGSP-1. Scan the QR code to view the animation or use the following web-link: <https://youtu.be/CceYR1NvAiM>

In both the capture cases that we discussed so far, we can see that out of SRP and STBE, the former has a more deciding effect on the motion of the particle when it is far away from the asteroid. The way the particles change their direction of motion is consistent with the direction in which the SRP perturbation is acting. So now we know how SRP is affecting a particle's motion while it is in a capture orbit around an asteroid. But now, we shall take a look at how these Solar perturbations are also responsible for creating a capture orbit in the first place.

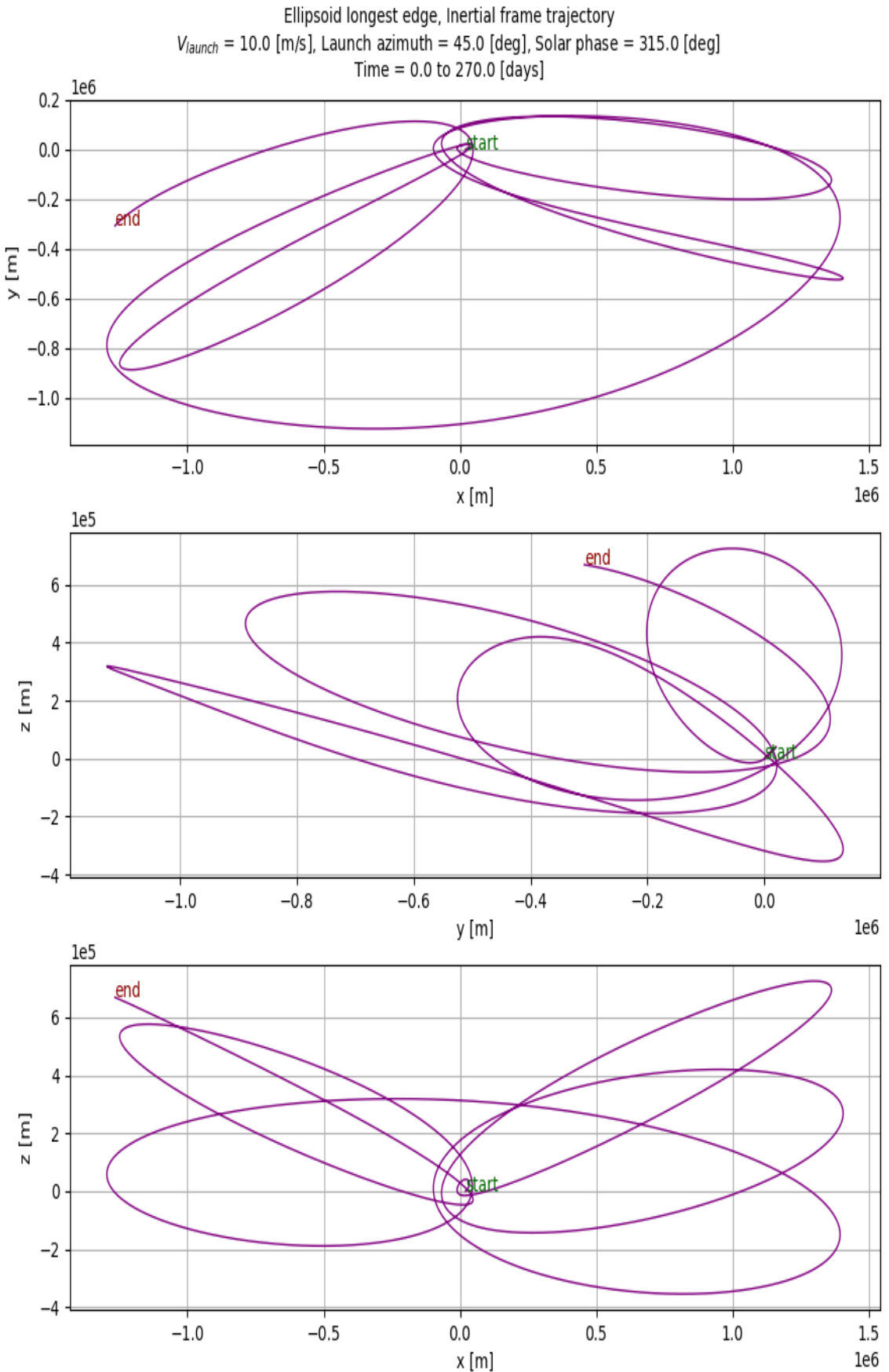


Figure 2.9: 2D inertial frame trajectory of capture regolith for case number 5 in Table 2.2. Particle code LoGSP-1.

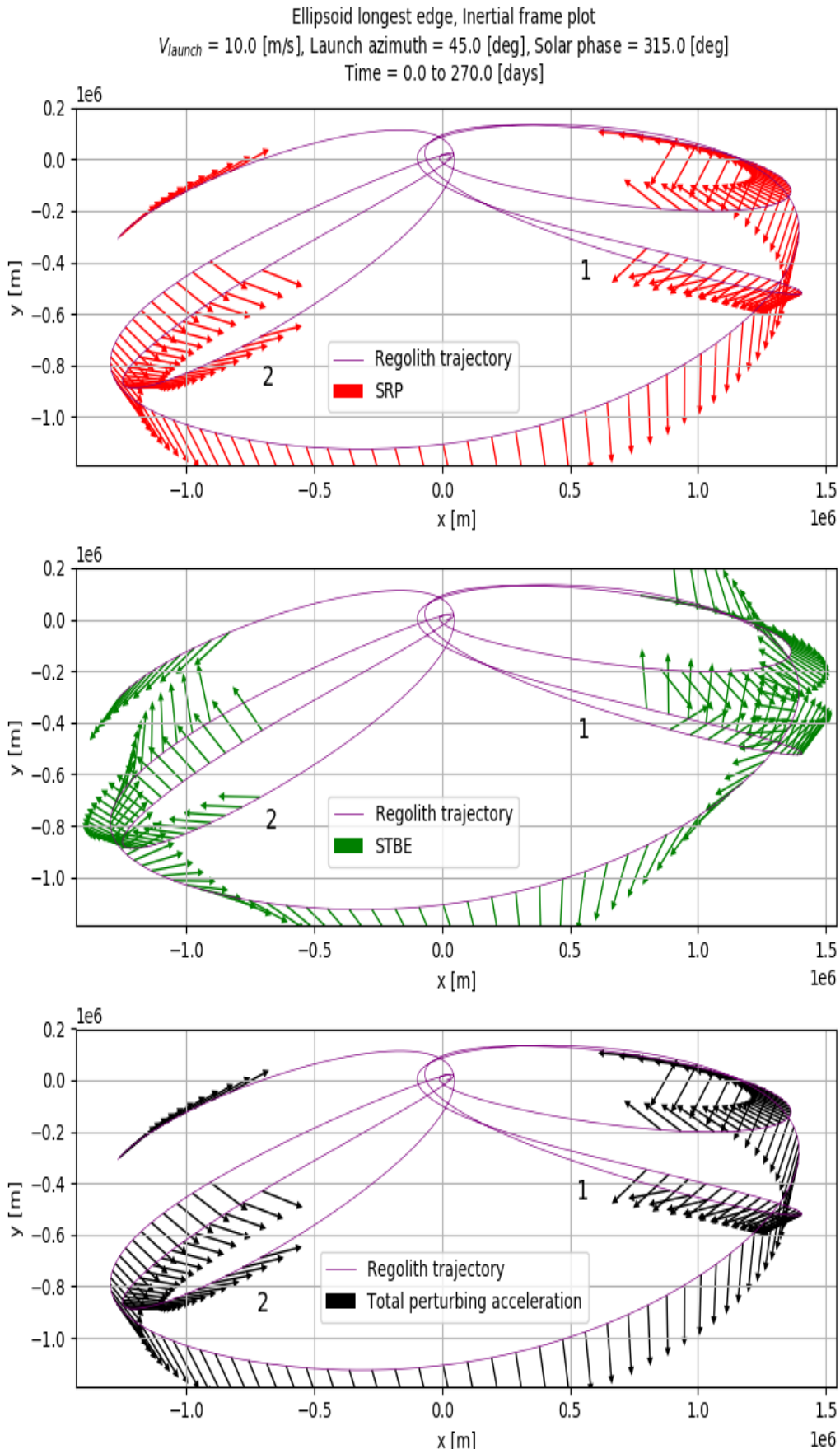


Figure 2.10: 2D trajectory of capture regolith for case number 5 in Table 2.2 with direction of SRP and STBE perturbation vectors along with the sum total of the two. Note that the vectors are shown only for those parts of the trajectory where the SRP magnitude is of the same order as that of the asteroid's gravitational acceleration. For those very same points along the trajectory, the magnitude of the STBE is always 1.0 order of magnitude smaller than the gravitational acceleration. Particle code LoGSP-1.

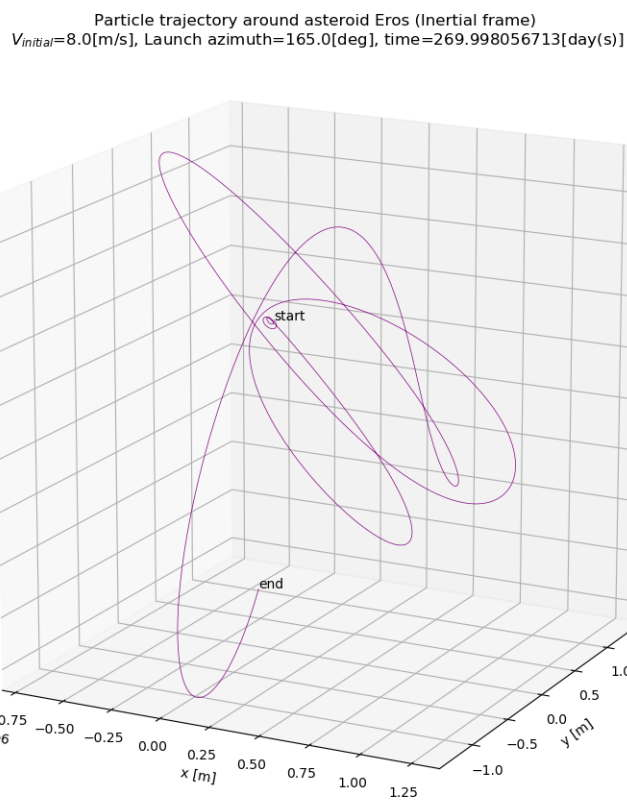
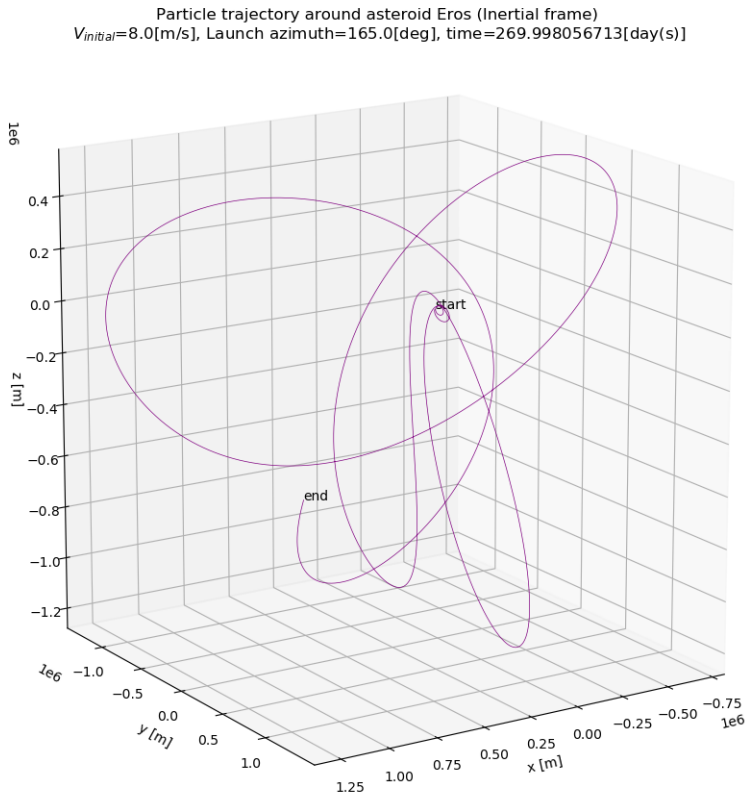


Figure 2.11: 3D inertial frame trajectory of capture regolith for case number 8 in Table 2.2 from two different viewing angles. Particle code LoGSP-1.

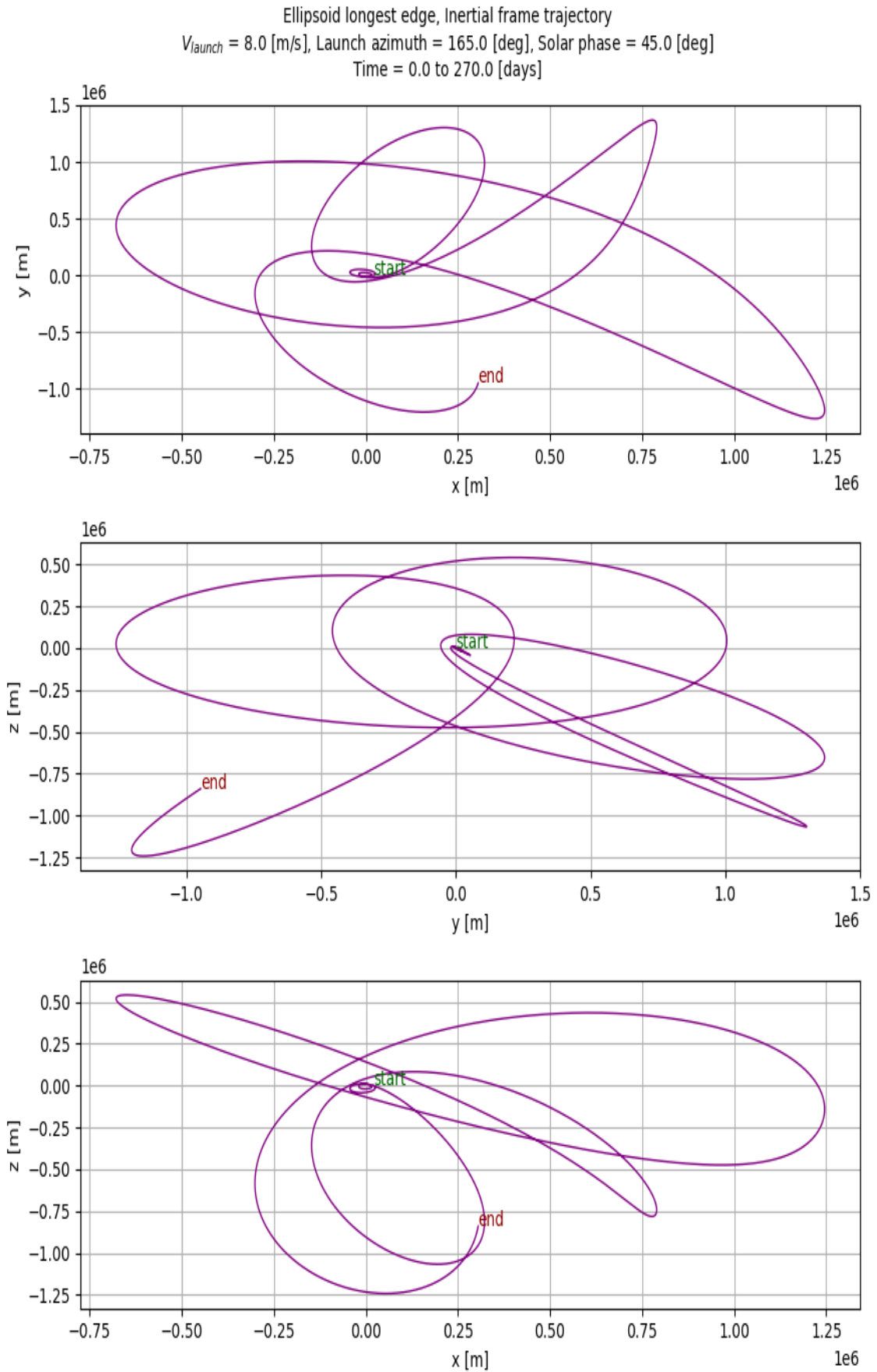


Figure 2.12: 2D inertial frame trajectory of capture regolith for case number 8 in Table 2.2. Particle code LoGSP-1.

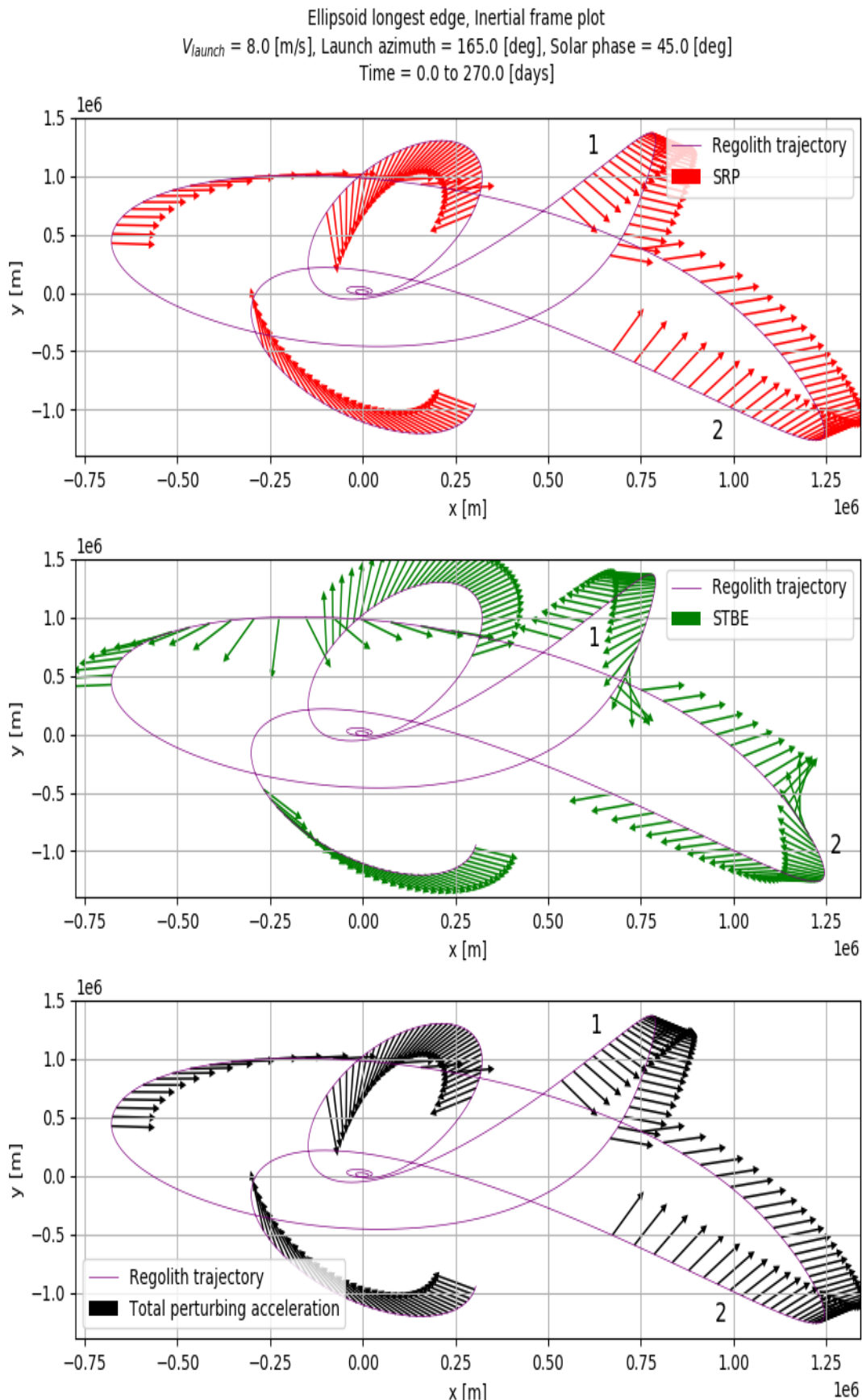


Figure 2.13: 2D trajectory of capture regolith for case number 8 in Table 2.2 with direction of SRP and STBE perturbation vectors along with the sum total of the two. Note that the vectors are shown only for those parts of the trajectory where the SRP magnitude is of the same order as that of the asteroid's gravitational acceleration. For those very same points along the trajectory, the magnitude of the STBE is always 1.0 order of magnitude smaller than the gravitational acceleration. Particle code LoGSP-1.

Let us begin with capture case number 8 in Table 2.2. Figure 2.15 shows two different trajectories for the particle launched with the same initial conditions. The one shown in dotted line is for the case when Solar perturbations were omitted from the simulation, which eventually results in the particle escaping the asteroid after 1.4 [days]. The one in the solid line shows the capture trajectory (actually a section of the entire capture trajectory as seen in Figure 2.12) when Solar perturbations were included in the simulation. Note that we show the perturbed trajectory (capture case) for the same amount of time (1.4 [days] instead of 270.0 [days]) as taken by the unperturbed trajectory (escape case) to be able to do a one-to-one comparison. The arrows plotted along this trajectory indicate the direction of the perturbing acceleration due to SRP. Figure 2.14 directs to an animation for both the unperturbed and perturbed trajectory.



Figure 2.14: 2D trajectory animation (XY Plane) of capture regolith for case number 8 in Table 2.2. Particle code LoGSP-1. Scan the QR code to view the animation or use the following web-link: <https://youtu.be/CdFKKR3UDJ0>

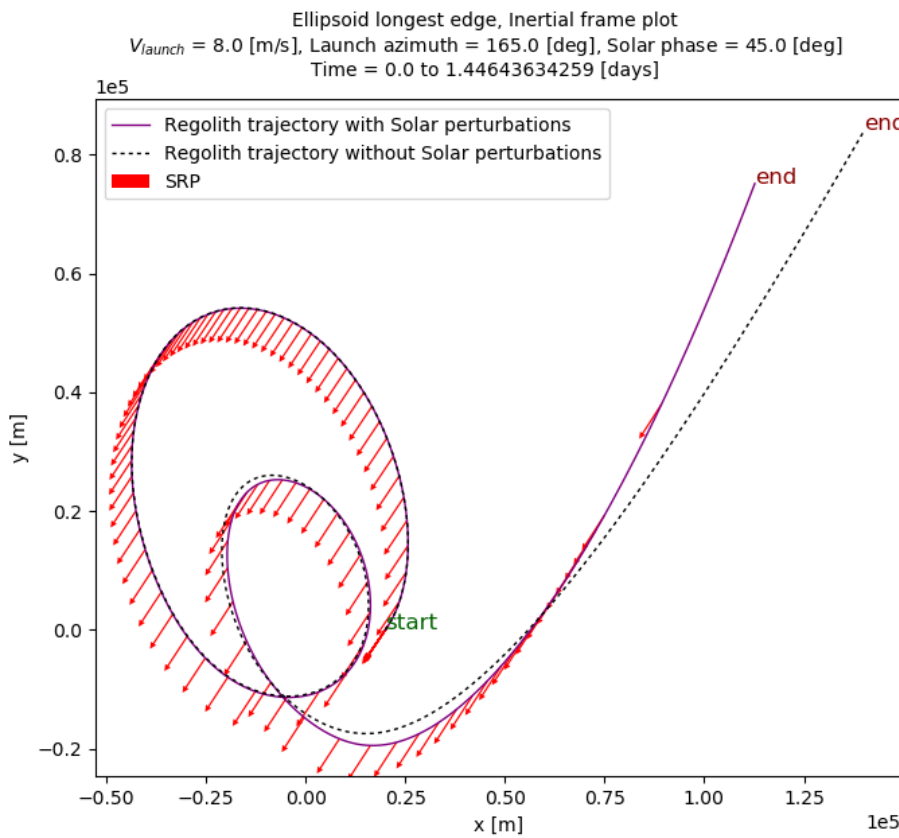


Figure 2.15: Inertial frame 2D trajectory (XY plane) of capture regolith for case number 8 in Table 2.2 with direction of SRP perturbation vector compared with the trajectory of a particle launched with the same initial conditions but in absence of Solar perturbations. Particle code LoGSP-1.

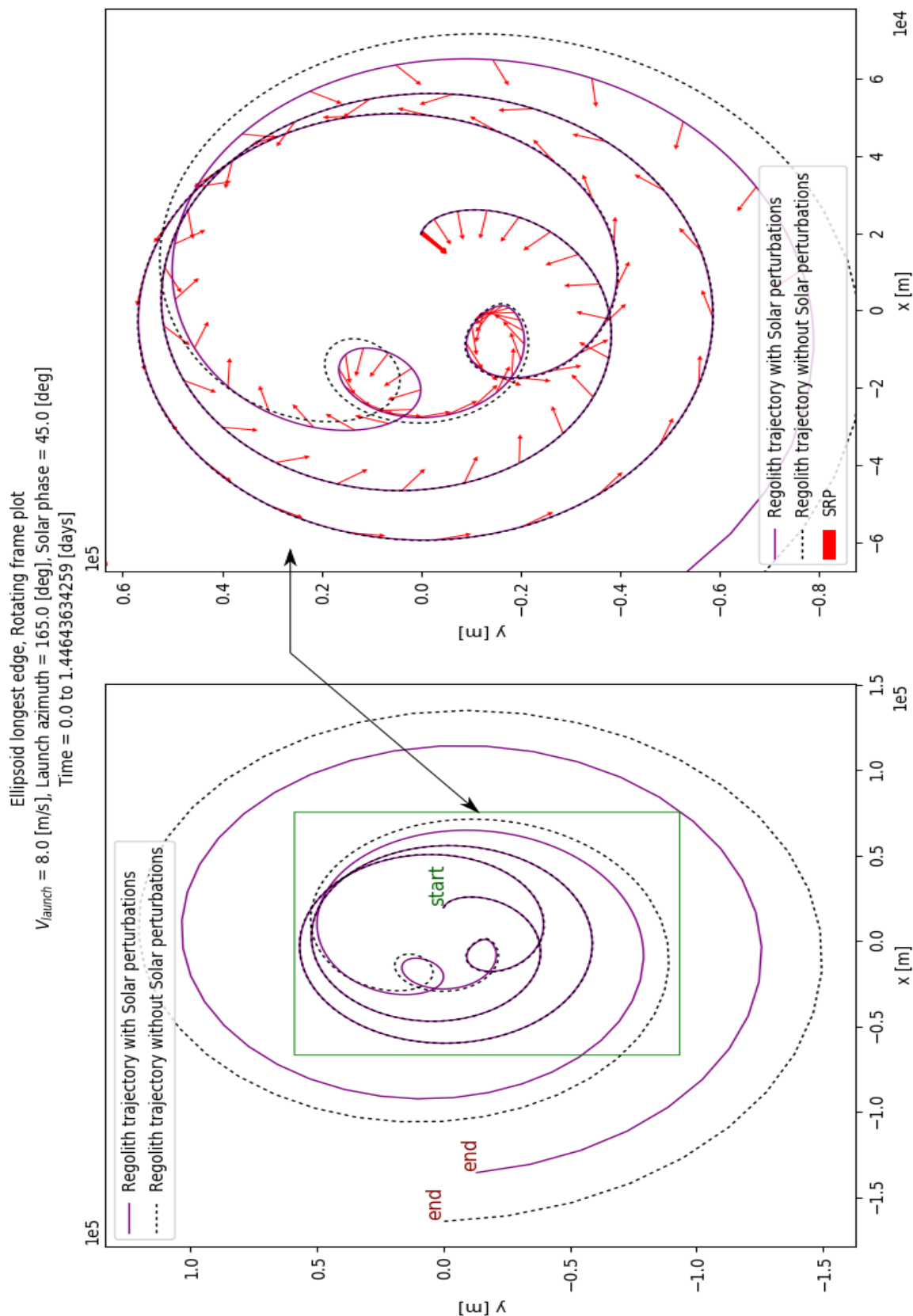


Figure 2.16: Rotating frame 2D trajectory (XY plane) of capture regolith for case number 8 in Table 2.2 with direction of SRP perturbation vector compared with the trajectory of a particle launched with the same initial conditions but in absence of Solar perturbations. Particle code LoGSP-1.

From the animation we can see that even as the particle has just been lofted from the surface of the asteroid, there are very subtle and minute differences, in the range to the particle and its velocity, between the perturbed and unperturbed trajectory. Ofcourse as the state vector differences are so small initially, the perturbed and unperturbed trajectory overlap with each other and can be seen so in Figure 2.15. Later, as the trajectory progresses, we see that these differences increase to a significant quotient because the effect of SRP adds up after a certain amount of time. A snippet from the trajectory animation in Figure 2.17 clearly shows the said differences. This snippet was taken around the moment when the perturbed and unperturbed trajectory start to separate from each other.

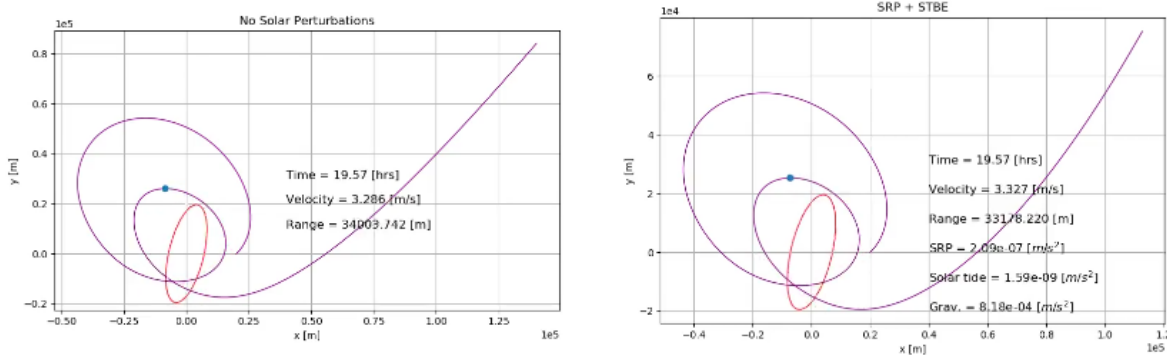


Figure 2.17: Animation snippet of the inertial frame 2D trajectory (XY plane) of capture regolith for case number 8 in Table 2.2. The trajectory on the left is for the case when Solar perturbations were omitted from the simulation and the trajectory on the right includes them. Note the differences in the range to the particle and its velocity for the same time stamp and rotational state of the asteroid. Particle code LoGSP-1.

In Figure 2.15 we can see that the departure in the perturbed trajectory from the unperturbed one is consistent with the direction in which the perturbing acceleration from SRP is acting. This can also be seen a bit more clearly when we look at the trajectory plot in the asteroid centric rotating frame or the body frame as shown in Figure 2.16. The plot on the left shows the trajectory for 1.4 [days] (i.e. until escape for the unperturbed trajectory) as viewed from the rotating frame, and the plot on the right zooms into a small part of this trajectory to show how SRP is responsible for changing the course of the particle. It is easily seen how the SRP vector pulls the trajectory away from the unperturbed one, thereby avoiding an escape scenario.

We see a similar effect when we look at capture case number 5 from Table 2.2. The inertial frame trajectory, both perturbed and unperturbed, for it are shown in Figure 2.18. With Solar perturbations removed from the simulation, the initial conditions for this particle result in it getting launched on a highly elliptical orbit and eventually crashing onto the surface of the asteroid. The particle, however, avoids this fate when Solar perturbations are included in the simulation. Just like before, we only show the SRP vector because it is more significant than STBE when the particle is near the asteroid (STBE is 5.0 orders magnitude smaller than gravitational acceleration compared to SRP which is only 3.0 orders of magnitude smaller when the particle is near the asteroid). Ofcourse, we see that the particle eventually moves far away from the asteroid but again we have discussed previously that the direction of SRP perturbing acceleration is enough to decide how the trajectory of the particle would behave. In Figure 2.18, it can be clearly seen that the direction of the perturbing acceleration due to SRP is consistent with how the trajectory departs from its unperturbed counterpart.

Ofcourse SRP is not directly responsible here, but rather indirectly, to get a capture orbit. The inclusion of SRP causes the regolith/particle trajectory to depart slowly from its unperturbed counterpart resulting in a different or rather favorable phasing (in this context we mean the location of the particle with respect to a given rotational state of the asteroid) which leads to the particle getting

trapped around the asteroid.

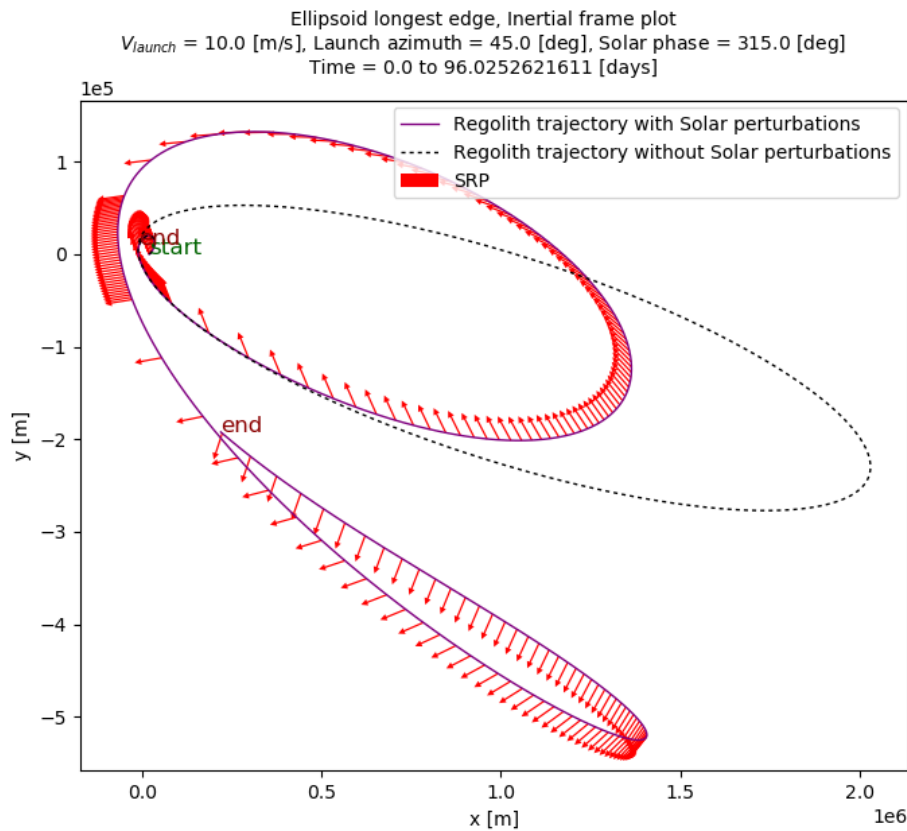


Figure 2.18: Inertial frame 2D trajectory (XY plane) of capture regolith for case number 5 in Table 2.2 with direction of SRP perturbation vector compared with the trajectory of a particle launched with the same initial conditions but in absence of Solar perturbations. Particle code LoGSP-1.

An example for this is shown in Figure 2.19.

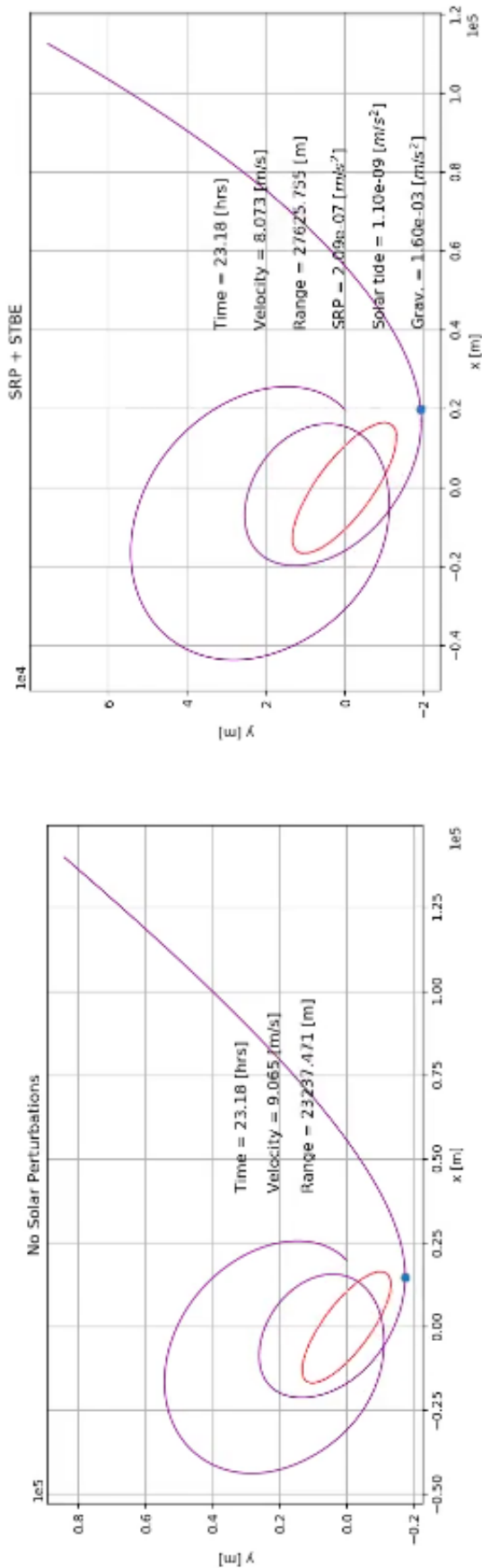


Figure 2.19: Animation snippet for an inertial frame 2D trajectory (XY plane) of capture regolith for capture case number 8 in Table 2.2. Particle code LoGSP-1.

BIBLIOGRAPHY

- [1] Garcia Yarnoz, Daniel, Sanchez Cuartielles, Joan-Pau, and McInnes, Colin R. "Passive sorting of asteroid material using solar radiation pressure". In: *Journal of Guidance, Control, and Dynamics* 37.4 (2014), pp. 1223–1235.
- [2] *Jet Propulsion Laboratory, Solar System dynamics, Asteroids*. Accessed 1 July 2016. URL: <http://ssd.jpl.nasa.gov/?asteroids>.
- [3] *Jet Propulsion Laboratory, Why Study Asteroids?* Accessed 1 July 2016. URL: http://ssd.jpl.nasa.gov/?why_asteroids.
- [4] Keller, Lindsay P and Berger, Eve L. "A Transmission Electron Microscope Investigation of Space Weathering Effects in Hayabusa Samples". In: (2014).
- [5] Marchis, F et al. "Multiple asteroid systems: Dimensions and thermal properties from Spitzer Space Telescope and ground-based observations". In: *Icarus* 221.2 (2012), pp. 1130–1161.
- [6] Margot, Jean-Luc et al. "Asteroid systems: binaries, triples, and pairs". In: *Asteroids IV. University Arizona Press, Tucson* (2015), pp. 355–374.
- [7] *Wikipedia, Iron-Nickel Alloy*. Accessed 30 April 2017. URL: https://en.wikipedia.org/wiki/Iron%E2%80%93nickel_alloy.

Appendices

A

EXTRA FIGURES

This appendix contains figures which are used to support the explanation of certain results, arguments and conclusions in the main part of the Thesis report.

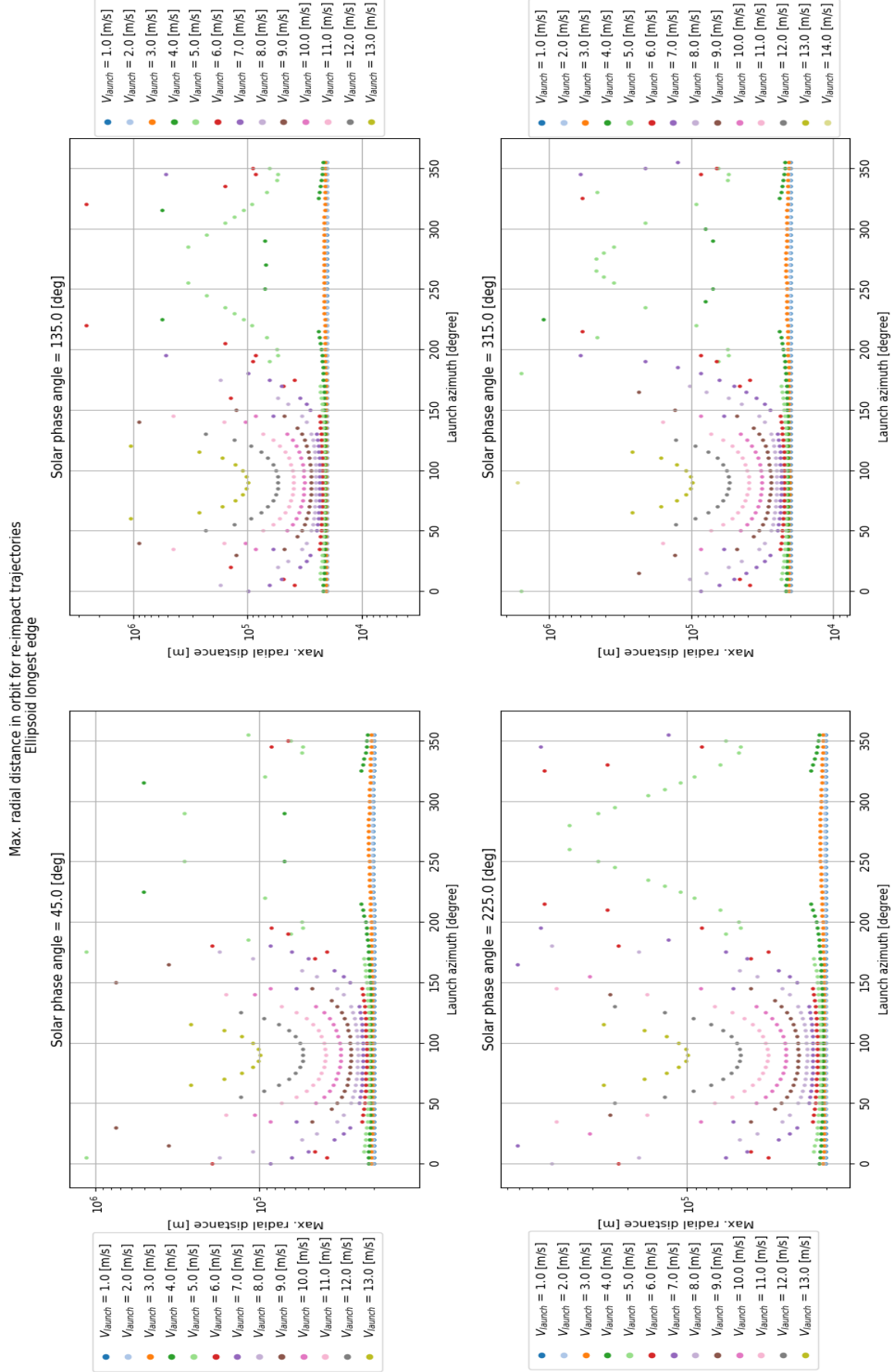
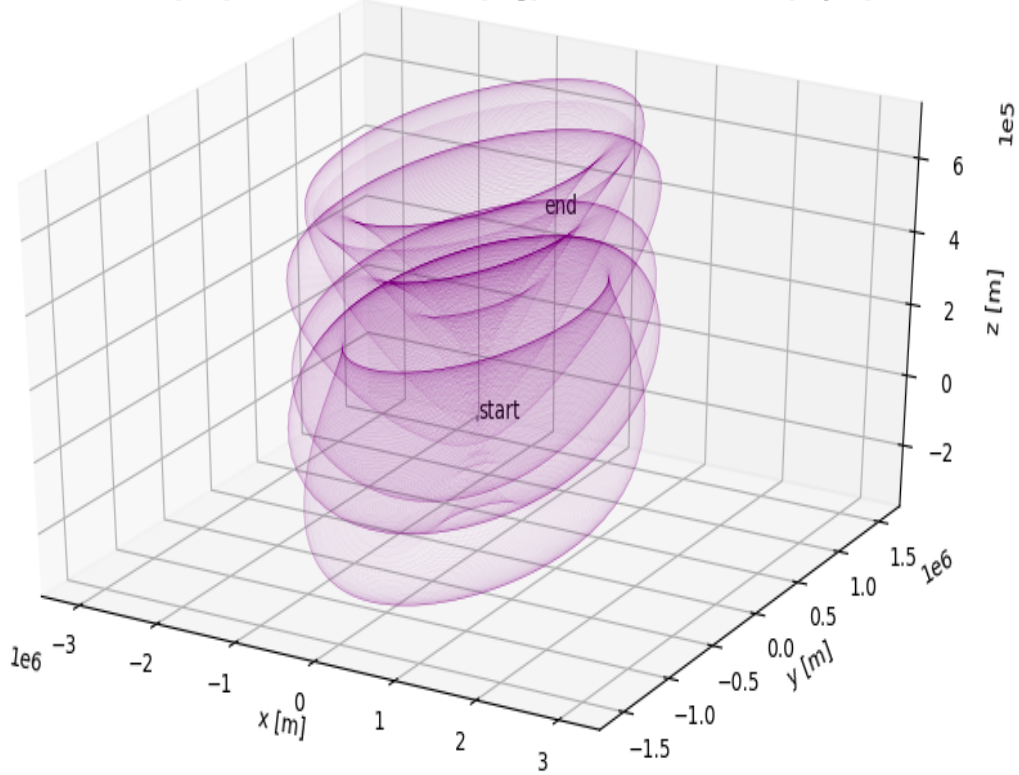


Figure A.1: Maximum radial distance (from the centre of the asteroid) attained by the regolith in orbit for different launch velocities and launch azimuths. The particles were launched from the longest edge of the ellipsoid (asteroid). Plots are for particle code LoGSP-1 and only for the re-impact scenario.

Particle trajectory around asteroid Eros (Body frame)
 $V_{initial}=10.0[\text{m/s}]$, Launch azimuth=45.0[deg], time=269.996608796[day(s)]



Particle trajectory around asteroid Eros (Inertial frame)
 $V_{initial}=10.0[\text{m/s}]$, Launch azimuth=45.0[deg], time=269.996608796[day(s)]

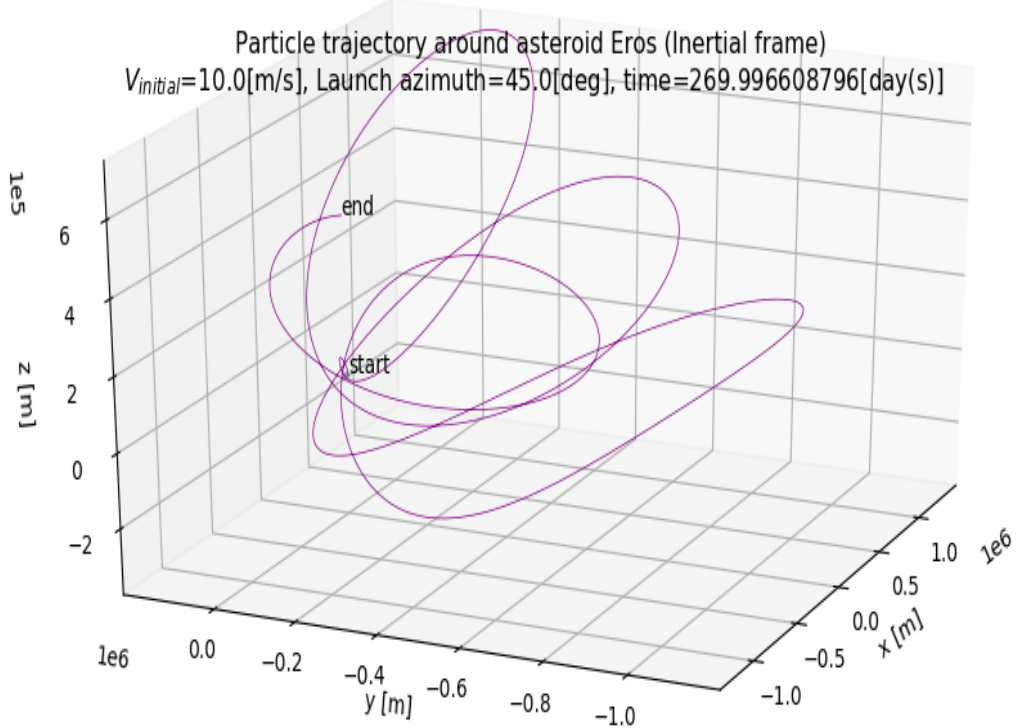


Figure A.2: 3D trajectory of capture regolith for case number 5 in Table 2.2. Particle code LoGSP-1.

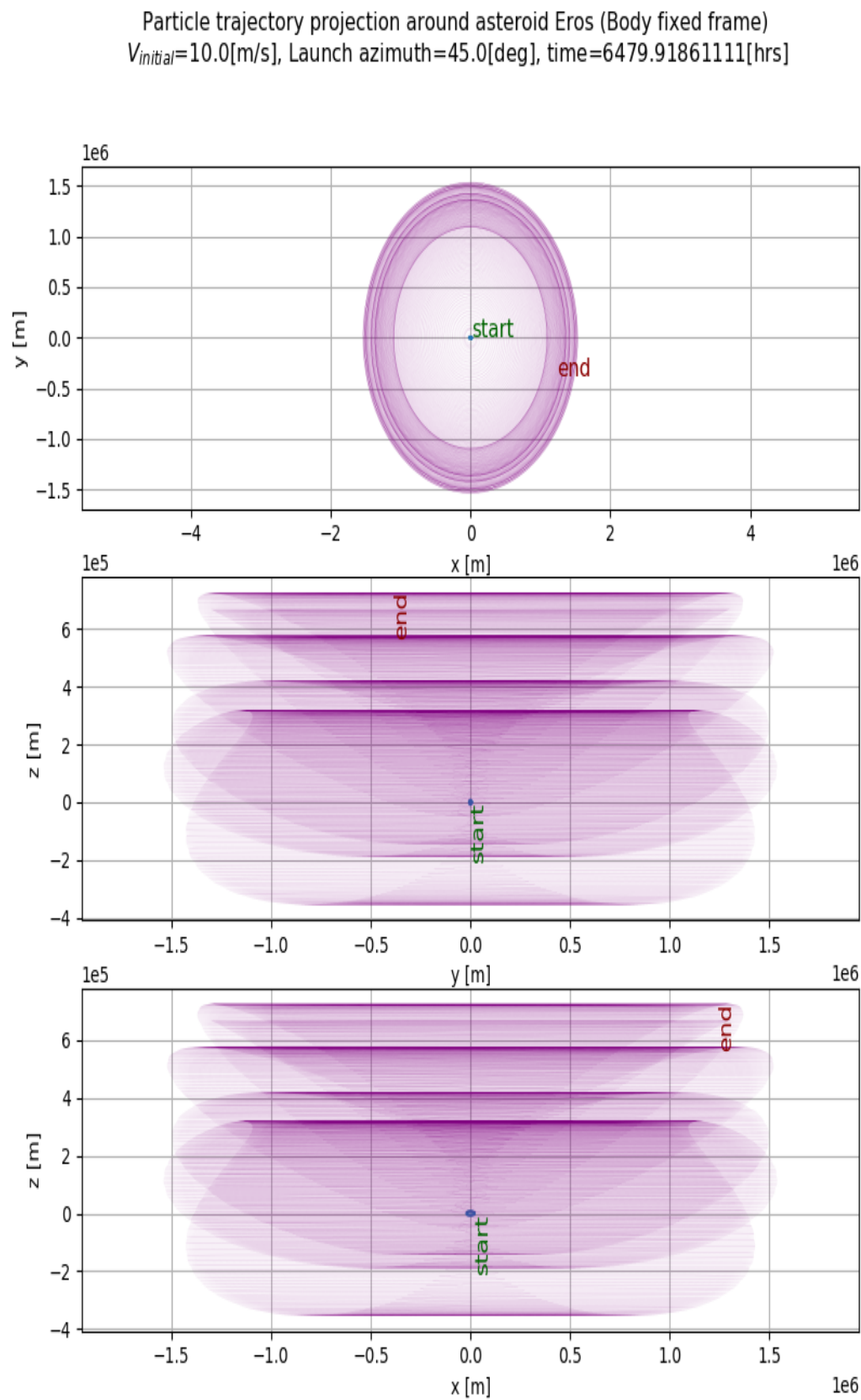


Figure A.3: 2D rotating frame trajectory of capture regolith for case number 5 in Table 2.2. Particle code LoGSP-1.

Particle trajectory around asteroid Eros (Body frame)
 $V_{initial}=8.0[\text{m/s}]$, Launch azimuth=165.0[deg], time=269.998056713[day(s)]

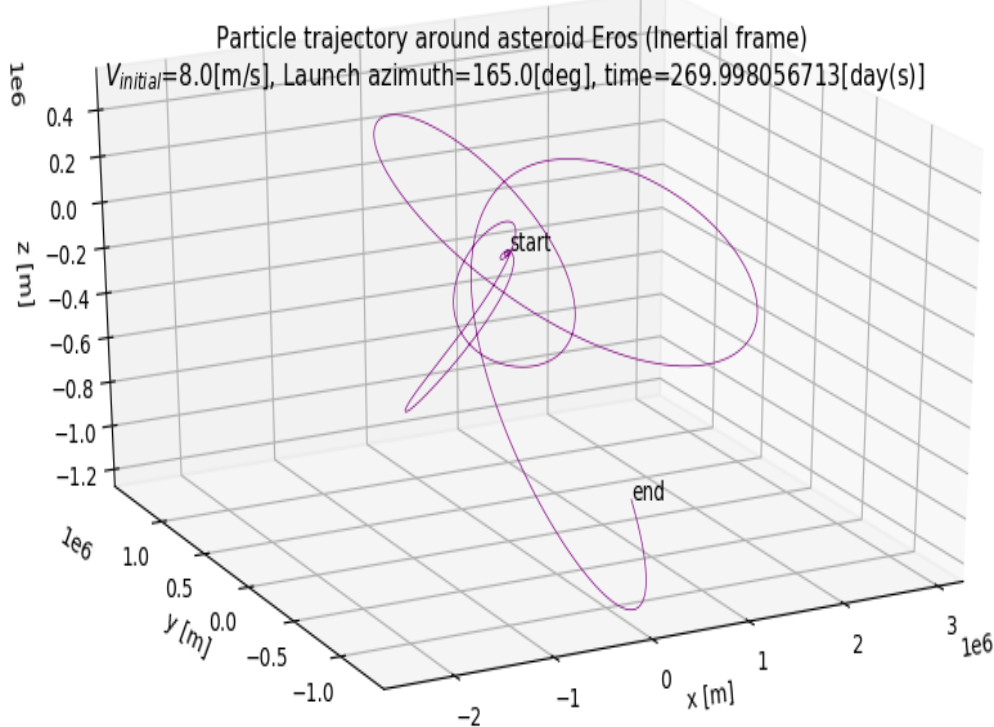
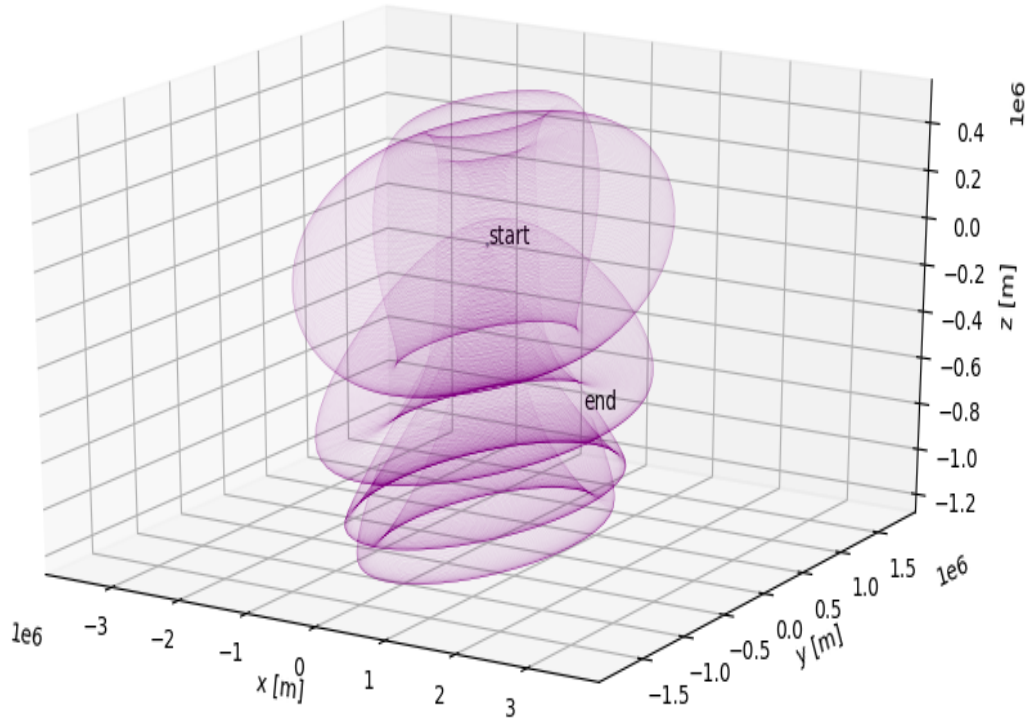


Figure A.4: 3D trajectory of capture regolith for case number 5 in Table 2.2. Particle code LoGSP-1.

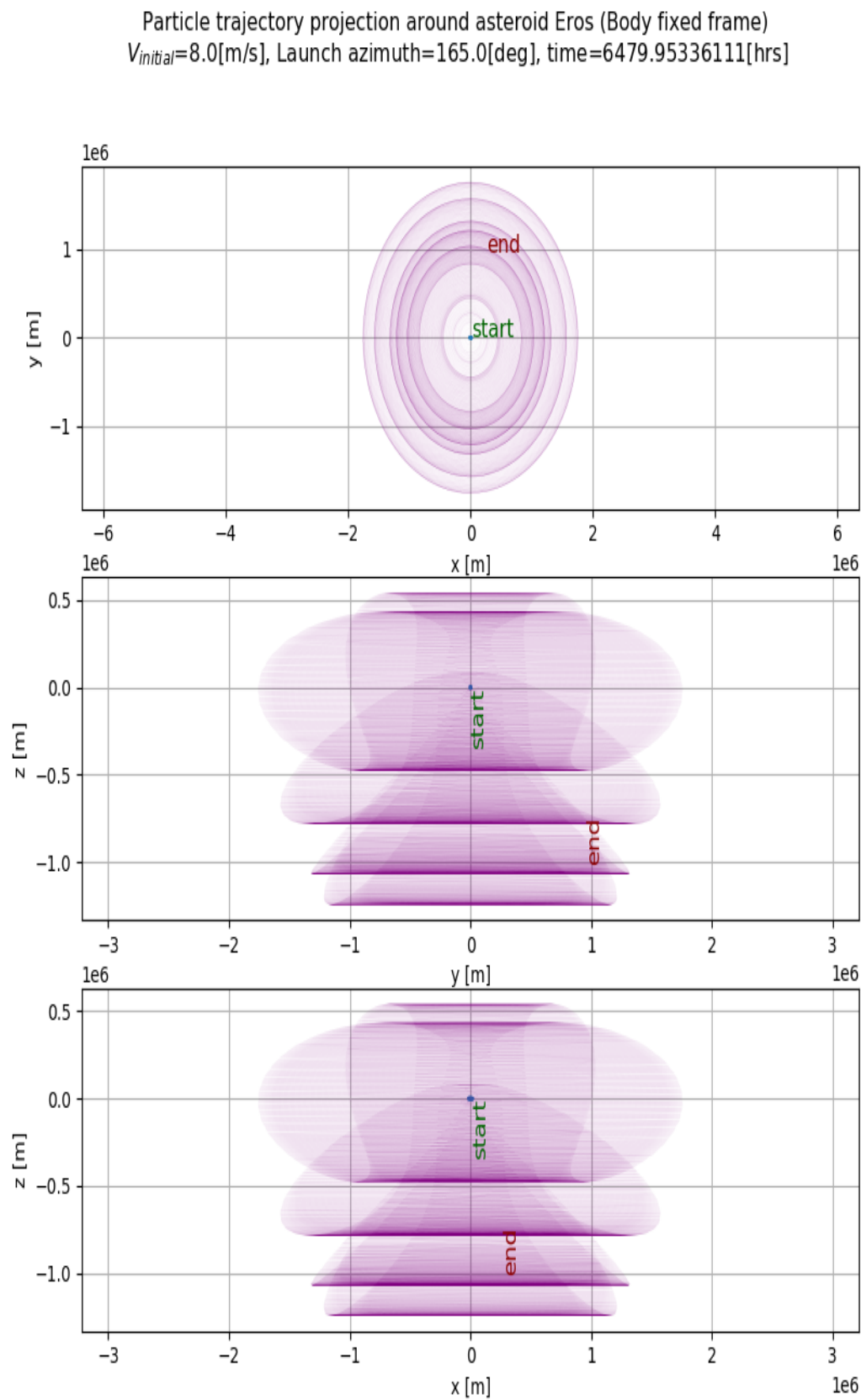


Figure A.5: 2D rotating frame trajectory of capture regolith for case number 8 in Table 2.2. Particle code LoGSP-1.